HYDROGEN DECREPITATION OF MAGNESIUM-RICH INTERMETALLICS

A THESIS SUBMITTED TO
THE GRADUATE SCHOOL OF NATURAL AND APPLIED SCIENCES
OF
MIDDLE EAST TECHNICAL UNIVERSITY

BY

ALPTEKİN AYDINLI

IN PARTIAL FULFILLMENT OF THE REQUIREMENTS
FOR
THE DEGREE OF MASTER OF SCIENCE
IN
MICRO AND NANOTECHNOLOGY

JULY 2013

Approval of the thesis:

HYDROGEN DECREPITATION OF MAGNESIUM-RICH INTERMETALLICS

submitted by **ALPTEKİN AYDINLI** in partial fulfillment of the requirements for the degree of **Master of Science in Micro and Nanotechnology, Middle East Technical University** by,

Prof. Dr. Canan Özgen _____
Dean, Graduate School of **Natural and Applied Sciences**

Prof. Dr. Tayfun Akın _____
Head of Department, **Micro and Nanotechnology**

Prof. Dr. Tayfur Öztürk _____
Supervisor, **Metallurgical and Materials Engineering Dept., METU**

Prof. Dr. Hüsnü Özkan _____
Co-supervisor, **Engineering and Architecture Fac., İstanbul Aydın Uni.**

Examining Committee Members:

Prof. Dr. Vedat Akdeniz _____
Metallurgical and Materials Engineering Dept., METU

Prof. Dr. Tayfur Öztürk _____
Metallurgical and Materials Engineering Dept., METU

Assoc. Prof. Dr. Caner Durucan _____
Metallurgical and Materials Engineering Dept., METU

Assist. Prof. Dr. Y. Eren Kalay _____
Metallurgical and Materials Engineering Dept., METU

Assist. Prof. Dr. Gülhan Çakmak _____
Metallurgical Engineering Dept., Bülent Ecevit University

Date: 12.07.2013

I hereby declare that all information in this document has been obtained and presented in accordance with academic rules and ethical conduct. I also declare that, as required by these rules and conduct, I have fully cited and referenced all material and results that are not original to this work.

Name, Last Name: Alptekin AYDINLI

Signature:

ABSTRACT

HYDROGEN DECREPITATION OF MAGNESIUM-RICH INTERMETALLICS

Aydınlı, Alptekin
M.Sc., Micro and Nanotechnology
Supervisor: Prof. Dr. Tayfur Öztürk
Co-supervisor: Prof. Dr. Hüsnü Özkan

July 2013, 66 pages

The production of metal hydride canisters may involve mechanical milling of the alloy powders under protective atmosphere and filling them into the canister in a glove-box environment. Such processes are often quite costly, and it is desirable to find a process which does not necessitate the use of protective atmosphere. Hydrogen decrepitation is one such process which involves in-situ pulverization of hydrogen storage alloys. The process starts with coarse alloy powders filled into a canister in open atmosphere and then subjected to several cycles of severe hydrogenation and dehydrogenation treatments which reduce the particles into submicron sizes. Two alloys were selected in the current study; Mg_2Ni and Mg_2Cu. The alloys were prepared by skull melting in an induction furnace using a cold crucible. Both Mg_2Ni and Mg_2Cu were melted under high pressure argon atmosphere due to high partial pressure of Mg. Solid alloys obtained in this way were pulverized by crushing them in a mortar and sieved to yield particles within 63-53 μm range. The alloy powders were then subjected to 10 hydrogenation cycles in a custom-made apparatus. Samples from hydrogenation cycles were examined by SEM, laser diffraction and BET analysis techniques so as to follow the decrepitation process. Results showed that Mg_2Ni alloy powder was pulverized easily upon cycling reaching to submicron sizes with no more than three hydrogenation cycles. Mg_2Cu, on the other hand, was resistant to pulverization. This was despite the fact that the alloy was dissociated upon hydriding to MgH_2 and $MgCu_2$ with 24.6% volume expansion.

Keywords: Hydrogen Storage, Metal Hydrides, Hydrogen Decrepitation, Mg_2Ni, Mg_2Cu

ÖZ

MAGNEZYUMCA ZENGİN MİKRON ALTI İNTERMETALİK PARÇACIKLARIN HİDRÜRLEME YÖNTEMİ İLE ÜRETİMİ

Aydınlı, Alptekin
Yüksek Lisans, Mikro ve Nanoteknoloji
Tez Yöneticisi: Prof. Dr. Tayfur Öztürk
Ortak Tez Yöneticisi: Prof. Dr. Hüsnü Özkan

Temmuz 2013, 66 sayfa

Metal hidrür tüplerinin üretimi, alaşım tozlarının kontrollü atmosferde öğütülmesi ve yine koruyucu atmosfer altında tüplere doldurulması ile gerçekleştirilebilir. Bu yöntemler genellikle çok pahalıdır ve koruyucu atmosfer gerektirmeyen farklı yöntemlerin kullanılması düşük maliyetli tüplerin üretimi açısından caziptir. Hidrürleme pulverizasyonu bu amaçla kullanılan bir işleme şekli olup nispeten kaba alaşım parçacıklarının açık atmosferde tüpe doldurulmasından ve takiben tüpün tekrarlı hidrürleme ve dehidrürleme çevrimine tabii tutulmasından ibarettir. Bu çalışmada iki alaşım seçilmiştir; Mg_2Ni ve Mg_2Cu. Alaşımlar basınç altında bir endüksiyon fırınına takılı soğuk potada üretilmiş, takiben havan içinde dövülerek toz haline getirilmiş ve 63-53 μm aralığında parçacıklar elde edilmiştir. Takiben tozlar, özel olarak tasarlanmış bir cihaza yerleştirilmiş ve 10 hidrürleme çevrimine tabii tutulmuştur. Hidrürleme çevrimi sonunda alınan numuneler taramalı elektron mikroskobu ile yapısal olarak, elde edilen parçacık büyüklüğü açsından da lazer kırınımı ve BET analizi teknikleri ile incelenmiştir. Sonuçlar Mg_2Ni'nin kolaylıkla pulverize olduğunu ve mikron altı boyutlara ulaşılması için 3 çevrimin yeterli geldiğini göstermiştir. Mg_2Cu ile yapılan deneyler ise bu alaşımın hidrürleme sonucunda % 24.6'lık bir hacim artışı göstermesi, ilave olarak MgH_2 ve $MgCu_2$ dönüşmesine karşın pulverizasyona karşı dirençli olduğunu ortaya koymuştur.

Anahtar Kelimeler: Hidrojen Depolama, Metal Hidrürler, Hidrürleme Pulverizasyonu, Mg_2Ni, Mg_2Cu

Dedicated to my family

ACKNOWLEDGMENTS

I wish to express my gratitude to my supervisor, Prof. Dr. Tayfur Öztürk for his guidance, caring, patience, and providing me with an atmosphere for doing research. I also appreciate my co-supervisor, Prof. Dr. Hüsnü Özkan for his valuable contributions to complete my thesis.

I would like to thank Assist. Prof. Dr. Gülhan Çakmak for her help and suggestions especially for particle size characterization and XRD studies.

Many thanks to Fatih Pişkin, Burak Aktekin, Necmi Avcı, Ramona Davoudnezhad, Ezgi Onur, and other friends in the Energy Storage Materials Laboratory for their help and contributions during the course of this thesis. Thanks also to my friends at the Department of Metallurgical and Materials Engineering and also Micro and Nanotechnology Program, METU; Saffet Ayık, Serkan Yılmaz, Yusuf Yıldırım, Önder Şahin, Atalay Özdemir, Fatih Uzgur and Serdar Görümlü.

Finally, I would also like to thank my family for their support and encouragement. They were always there cheering me up and stood by me throughout the good times and the bad.

TABLE OF CONTENTS

LIST OF TABLES

TABLES

LIST OF FIGURES

FIGURES

CHAPTER 1

INTRODUCTION

Currently, there is much need for an efficient, economical and safe storage of hydrogen. Among the various alternatives, metal hydride storage is the best option regarding the volumetric storage capacity and safety factors. Owing to these advantages, canisters based on metal hydrides are the preferred options for mobile as well as stationary applications.

Production of metal hydride canisters generally involves mechanical milling of the alloy powders under inert atmosphere and charging these powders into the canister again under inert atmosphere as in glove-box environment. Mechanical milling techniques as well as handling of powders in glove-box environment are expensive processes. Thus there is a need to find a cost-effective method for the processing and handling the hydrogen storage alloys. Processing of powders via hydrogen decrepitation is one such alternative.

Hydrogen decrepitation is a well-known processing technique used for the production of magnets (e.g. Takeshita 1995) and in other metallurgical applications (e.g. Yoshimura and Nakahigashi 2002). But in general this technique has been considered as a side issue in metal hydrides. In this study, hydrogen decrepitation was examined as processing technique for the production of metal hydrides. The process begins with coarse alloy powders charged into a canister in open atmosphere and continues with several cycles of hydrogenation and dehydrogenation treatments.

In the current study two intermetallic alloys were selected; Mg_2Ni and Mg_2Cu. The alloys are similar to each other in that both are intermetallics. But they differ in the way that they hydrogenate. Mg_2Ni is hydrided directly to Mg_2NiH_4 with the volume expansion of 32.1%. In contrast, Mg_2Cu is subject to disproportionation reaction, i.e. upon hydrogenation it dissociates into $MgCu_2$ and MgH_2 with a volume expansion of 24.6%. Upon dehydrogenation MgH_2 and $MgCu_2$ combine again to form of Mg_2Cu. These latter reactions are similar reactions observed in hydrogenation-decomposition-desorption-recombination (HDDR) process which is often applied to magnet alloys.

CHAPTER 2

LITERATURE REVIEW

2.1 Hydrogen Storage Methods

In all chemical fuels, hydrogen has the highest heating value per mass. In addition, it is environmentally friendly and can be regenerated. At the present time hydrogen is not the primary fuel for world's energy consumption. There are two reasons for this situation. The first is that hydrogen is only a carrier of energy. Since hydrogen is solely found in the form of water and hydrocarbons on earth, it has to be extracted even though it is the most abundant element ever known. The second reason is that hydrogen is in the gas form at room temperature whose volumetric and gravimetric storage densities are critical for stationary and especially mobile applications (Züttel 2004).

Various techniques can be used for hydrogen storage: i) high pressure gaseous hydrogen, ii) liquid hydrogen, iii) hydrogen stored in porous media, iv) complex hydrides v) metal hydrides (Züttel 2004). Technical data of these methods taken from Züttel (2004) are tabulated in Table 2.1.

Table 2.1 Technical data of hydrogen storage methods. ρm: the gravimetric density, ρv: the volumetric density, T: working temperature, RT : room temperature (25 °C), p: pressure (Züttel 2004).

Storage method	**ρ_m (mass %)**	**ρ_v (kg H_2 m^{-3})**	**T (°C)**	**P (bar)**
High pressure gaseous hydrogen	13	<40	RT	800
Liquid hydrogen	Size dependent	70.8	-252	1
Hydrogen stored in porous media	≈2	20	-80	100
Complex hydrides	<18	150	>100	1
Metal hydrides	≈2	150	RT	1

High pressure gaseous hydrogen is the most preferred storage technique due to its technical simplicity and fast filling-releasing rate. The pressure should be high enough to reach reasonable storage densities. According to von Helmolt and Eberle (2007) when

factors including compression energy demand, driving range, infrastructure investment and others are taken into account, the ideal pressure for mobile hydrogen systems is around 35 MPa-70 MPa. Thus in a refueling station, the pressure of hydrogen is generally 40 MPa-75 MPa in order to refuel hydrogen directly and quickly by using the pressure difference. Storage vessel is the most important part in this form of hydrogen storage (Zheng et al. 2012).

Liquid hydrogen is quite attractive for on-board hydrogen storage systems because of its high densities. The density reached in the liquid is 800 times the density of the gas at atmospheric conditions. High pressurization is not a requirement in this method. Hence; despite of the necessary thermal insulation, liquid hydrogen storage tanks are lighter than the tanks which are chosen for other techniques. Moreover extreme pressure and/or temperature cycles are not applied to fill and empty the tanks. On the other hand, the method has the disadvantage that the liquefaction is an energy intensive process (Ewald 1998). Novel liquid hydrogen tanks can limit the heat flow to a few Watts/second and thus liquid hydrogen evaporates just a few percent per day (Mori and Hirose 2009).

In **the hydrogen storage in porous media,** the most important issues are the choice of appropriate adsorbent and operating conditions. In early times there was studies declared 60 wt.% content of hydrogen at ambient temperature and 112 bar pressure in carbon nanofibers and of 14-20% in alkali doped carbon nanotubes at temperatures from ambient to 400 °C and 1 bar pressure. Hence carbons as hydrogen storage materials have been attracted much interest. However, these extreme capacities have been discussed on fundamental grounds problems such as moisture contamination problem have emerged. Then much more moderate capacities which are less than 5 wt.% hydrogen at cryogenic conditions of 77 K have been published (Bhatia 2006).

Apart from carbon structures metal-organic frameworks (MOFs) are another promising materials for hydrogen storage. According to Suh et al. (2012) MOFs are crystalline materials with micropores (<2 nm) and channels formed by organic ligands which keeps metal ions together. A variety of MOF materials with surface areas from relatively small value to very large ones have been produced. In the literature one of the highest total hydrogen storage capacity was reported for MOF-210, the value being is 17.6 wt.% at 77 K and 80 bar (Furukawa et al. 2010).

Complex hydrides are hydrogen storage system where light elements sodium, lithium and beryllium can react with hydrogen to form complex compounds. For instance $LiBH_4$ can store 18 wt.% hydrogen. In addition alanates, amides, imides and borohydrides has attracted considerable attention as complex hydrides. Particularly alanates and borates are attractive due to their capacity for large quantity of and their light weight. However, dehydriding process in most of these compounds occurs in more than one step (Sakintuna et al. 2007).

Complex compounds such as $NaBH_4$ and ammonia borane (H_3NBH_3) are regenerative compounds, i.e. after release of hydrogen; a regeneration treatment has to be applied to convert the material back to the starting form. According to Hsueh et al. (2009) $NaBH_4$ release hydrogen and is regenerated with respect to the following reactions.

$$NaBH_4 + 2H_2O \rightarrow 4H_2 + NaBO_2 \quad (1)$$

$$NaBO_2 + 2Mg + 2H_2 \rightarrow NaBH_4 + 2MgO \quad (2)$$

In Figure 2.1 a regeneration scheme of ammonia borane proposed by Tumas et al. (2006) is shown.

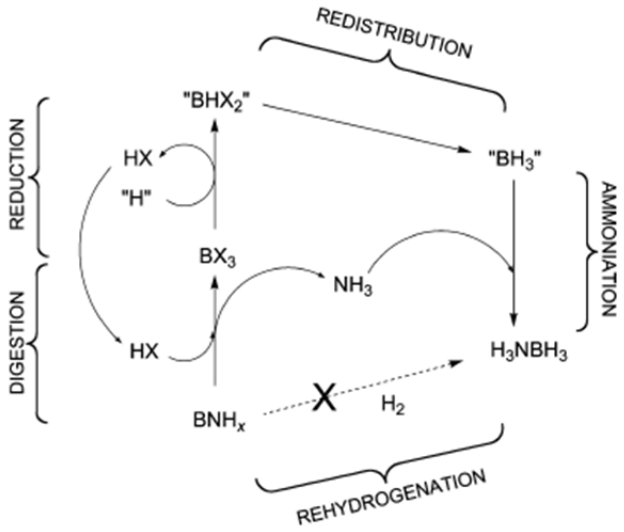

Figure 2.1 Regeneration scheme of ammonia borane (Tumas et al. 2006)

According to Metin et al. (2010) recently, ammonia borane complex has been realized as one of the most promising materials for hydrogen storage due to its high hydrogen capacity (19.6 wt.%), high stability under normal fuel cell reaction circumstances, and nontoxicity. Metin et al. (2010) also synthesized nickel nanoparticles as catalysts for dehydrogenation of ammonia borane.

The use could also be made of Na and Li as hydrogen storage media similar to the previous regenerative examples. These metals react with water and release hydrogen. According to Züttel (2004) gravimetric hydrogen density of sodium is 3 wt.% while the capacity with

lithium is much higher reaching 6.3 wt.% hydrogen. In this storage technique the reversibility and the control of the thermal reduction process are the major difficulties.

Metal hydrides have two main components which are metal atoms as host lattice and hydrogen atoms occupying interstitial sites, e.g. lattice defects. Hydrogen atoms can be trapped by a vacancy or a line defect in a metal lattice. Hydrogen atoms may align along a line defect in the form of a string. Such a structure increases the lattice stress, particularly if two adjacent atoms recombine to form molecular hydrogen. Synthesis of metal hydrides is possible in the light of two reactions: direct dissociative chemisorption and electrochemical splitting of water which are seen below.

$$M + X/2H_2 \leftrightarrow MH_X \tag{3}$$

$$M + X/2H_2O + X/2e^- \leftrightarrow MH_X + X/2OH^- \tag{4}$$

Here M represents the metal. In electrochemical reaction a catalyst such as palladium has to be included to break down the water (David 2005).

Both necessary thermodynamic and kinetic circumstances must be fulfilled for hydrogen storage. In the situation of appropriate circumstances, a metal under a hydrogen atmosphere absorbs hydrogen until equilibrium is reached. There are several reaction steps which kinetically may prevent a hydrogen storage system to reach its thermodynamical equilibrium within a certain time. Thus the reaction rate of a metal–hydrogen system depends on pressure and temperature (David 2005).

Metal and hydrogen generally form two different types of hydrides, α-phase and β-phase hydride. Only some amount of hydrogen adsorbs in α-phase but in β-phase the hydride is completely formed. In Figure 2.2 a schematic of phase transition is shown. When hydrogen is exposed to a metal, it diffuses from the surface of the metal to the phase-transition interface trough the β-phase and forms fresh β-phase hydride. In the case of desorption, hydrogen diffuses from the phase-transition interface to the surface of the metal through the α-phase and finally it is recombined in the form of molecular hydrogen (David 2005). In the following section metal hydrides will be classified and discussed with details.

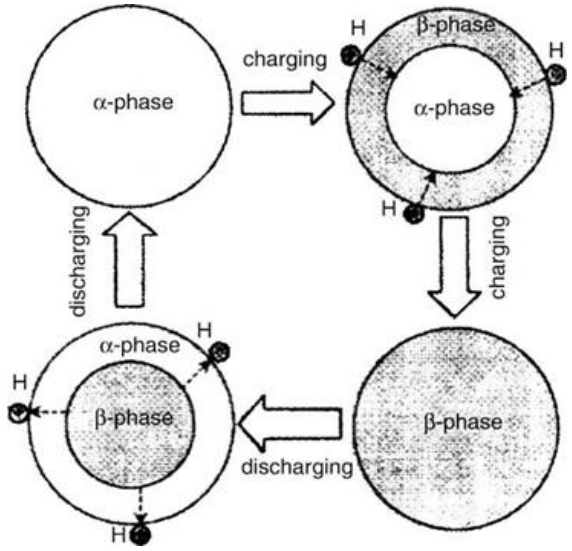

Figure 2.2 Schematic drawing of metal hydride phase transition (David 2005).

2.2 Hydrogen Storage in Metal Hydrides

Since hydrogen is a highly active element it can form variety of hydrides and solid solutions with metal and alloys. In Figure 2.3 a hydride 'family tree' of the elements, alloys and complexes depicted by Sandrock (1999) is seen.

As seen in the figure there are two main groups of hydrides in the family; alloys and complexes. Here complex hydrides are already reviewed above. Among alloys, the most important group is intermetallics; where they form a variety of subgroups involving elements A and B e.g. AB_5, AB_2, AB, A_2B etc. Here A is the element forming a strong hydride and B is relatively inert to hydrogen. In this section only AB_5, AB_2 and A_2B type alloys will be reviewed.

The prototype for **AB_5** compounds is $LaNi_5$. Here La as mentioned above has a strong affinity to hydrogen forming LaH_3 and Ni is relatively inert to hydrogen. The crystal structure of $LaNi_5$ is hexagonal (Pearson symbol: hP6 and space group: P6/mmm). Sandrock (1999) reported that maximum hydrogen capacity of $LaNi_5$ is 1.49 wt.%.

Sandrock (1999) also reported that AB_5s were first recognized by chance while working on $SmCo_5$ magnet alloys. Since various elements can be substituted (at least partially) into the A and B lattice sites, AB_5 class has a significant versatility. A elements are usually Ca, Y, Zr etc. or one or more of the lanthanides (at. no. 57–71). The main B element is Ni but a variety of other elements are possible such as Co, Al, Mn, Fe, Cu, Sn, Si, Ti, etc. Commercial AB_5

alloys are generally based on mischmetal (Mm=a mixture of Ce,La,Nd and Pr) for the A elements and Ni+Al+Mn+Co… for the B elements.

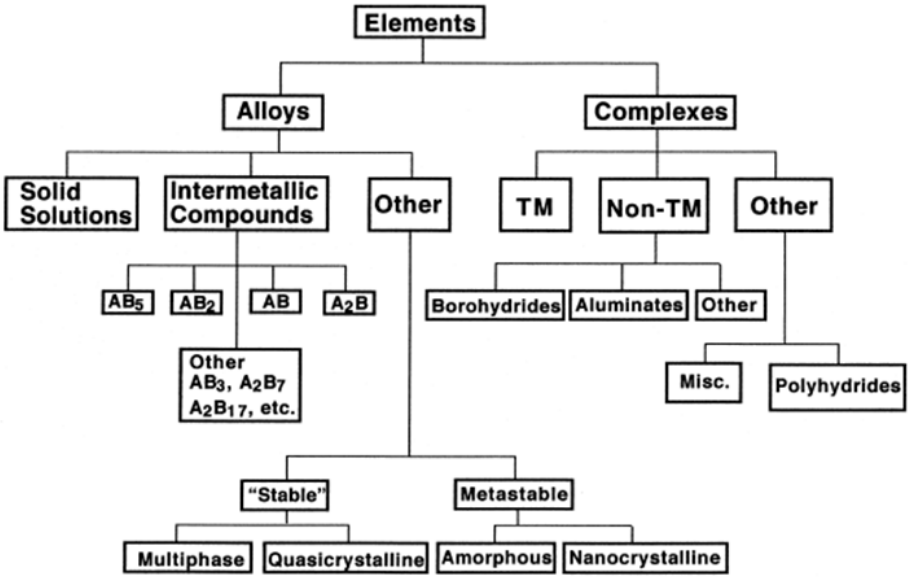

Figure 2.3 Family tree of hydriding alloys and complexes (TM represents transition metal) (Sandrock 1999).

The activation of AB_5 alloys is facile and rarely needs any heating. These alloys decrepitate after the first hydriding-dehydriding cycle to fine powder. In order to prevent oxidation of this slightly pyrophoric powder, safety precautions must be taken. AB_5 metallurgy is rather straightforward and virtually single phase alloy can be produced relatively easily in significant commercial quantities by vacuum induction melting (Sandrock 1999).

The **AB_2** class compounds are based on the Laves phase crystal structures. Ti and Zr are the main two elements on the A side for potential AB_2s. The B elements are usually chosen from different combinations of 3d atoms such as V, Cr, Mn and Fe (Sakintuna 2007). Both hexagonal and cubic Laves phase structures are possible. For example, $ZrMn_2$ has hexagonal C14 Laves phase structure (Pearson symbol: hP12 and space group: $P6_3/mmc$). $NbCr_2$ has cubic C15 Laves phase structure (Pearson symbol: cF24 and space group: Fd-3m).

It can be also mentioned that Ti-based alloys of AB_2 type alloys are multiphase alloys formed by BCC and Laves phases. Hydrogenation is affected by both of these phases. Indeed, the BCC and Laves phase have the same equilibrium pressure. Because of this

reason, this type of alloys are named Laves phase-related BCC solid solution (Hirscher 2010).

Compounds with Laves phase have been popular since late 90s through their reasonable hydrogen storage capacity. In comparison to $LaNi_5$ based alloys most of Laves phase alloys exhibit relatively high capacities, longer life, faster kinetics and relatively low cost. However, at room temperature AB_2 type hydrides are highly stable. Moreover these types of alloys are usually more sensitive under reactive gas atmospheres than the AB_5 type alloys. Hence, AB_2s can be poisoned by oxygen easily while it diminishes the storage capacity of AB_5s slightly (Sakintuna et al. 2007).

A_2B class alloys can have different types of crystal structures and are divided into subclasses. In one subclass e.g. Ti_2Ni, group 4A elements such as Ti, Zr or Hf occupy the A side and the B elements are transition metals, essentially Ni. Another subclass is based on Mg_2Ni which was first studied in the late 1960s by Reilly and Wiswall (1968). Since this study Mg_2Ni has been subjected to numerous investigations based on both fundamental and applications points of view (Sandrock 1999). Both Mg_2Ni and Mg_2Cu which were chosen for this study are reviewed below.

Mg combines with Ni in the form of two different intermetallic alloys, Mg_2Ni and $MgNi_2$. According to Reilly and Wiswall (1968), Mg_2Ni reacted readily with hydrogen (at a temperature of 325 °C at an H_2 pressure of 21 bar). On the contrary, $MgNi_2$ did not react with H_2. Although the rate of hydriding reaction was slow at the beginning, the kinetics improved noticeably after several hydriding/dehydriding cycles. Through these cycles, the Mg_2Ni reacted with hydrogen easily at temperatures as low as 200 °C and an H_2 pressure as low as 14 bar. Several pressure-composition isotherms for the Mg_2Ni-H_2 system taken from Riley and Wiswall (1968) are shown in Figure 2.4.

On the basis of the stoichiometry of the system and X-ray experiments Reilly and Wiswall (1968) revealed the reaction of Mg_2Ni with H_2 in the plateau region as the reaction below.

$$Mg_2Ni + 2H_2 \leftrightarrow Mg_2NiH_4 \quad (5)$$

The appearance of product of this reaction was nonmetallic and rust-colored. Short time air exposures did not affect the product but when it was stored for several months in a container such as stoppered bottle, the hydride was oxidized as its color started to turn into black. Reilly and Wiswall (1968) also determined density of the product as 2.57 g/cm^3.

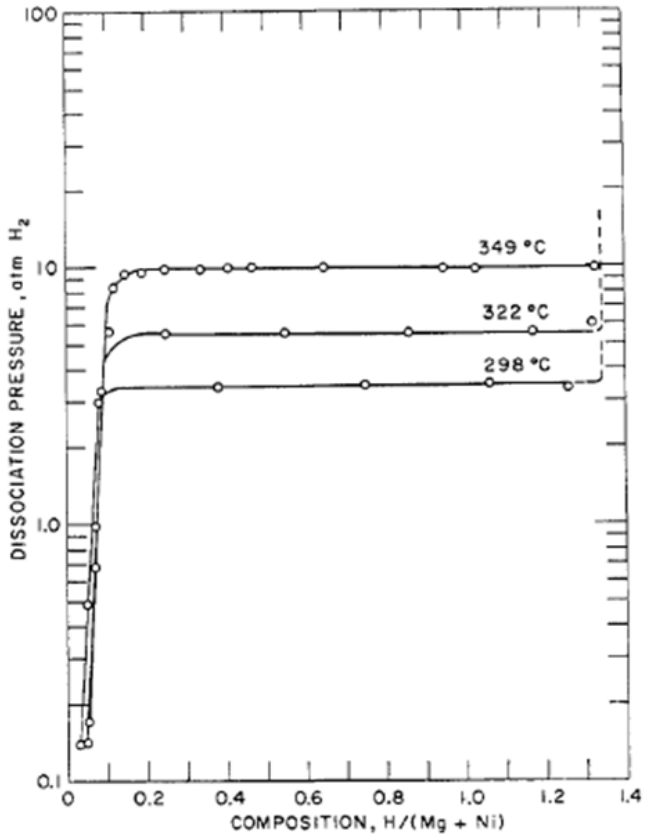

Figure 2.4 Pressure-composition diagram of the Mg_2Ni-H_2 system (Reilly and Wiswall 1968).

Mg_2Ni has a hexagonal crystal structure (Pearson symbol: hP18, space group: $P6_222$) with cell parameters; a=0.52 nm, b= 1.32 nm (Post et al. 1985). According to Orimo and Fujii (2001) Mg_2Ni can store 3.6 wt.% hydrogen in the form of Mg_2NiH_4 which has a covalent-type bonding consisting of Mg^{2+} and $[NiH4]^{4-}$ complex. In comparison with commercial $LaNi_5$ based alloys, hydrogen storage capacity of Mg_2Ni is about 3 times higher. However due to its covalent-type bonding, the enthalpy of hydride formation of Mg_2NiH_4 is −32.3 kJ/mol H which is at the same level with MgH_2. Also the dehydriding temperature is rather high, 520–570 K.

Mg_2Ni are attractive in terms of its cost and also in terms of hydrogen that it could store but desorption temperatures are too high for most applications. The stability of Mg_2NiH_4 is not influenced much by ternary and higher-order substitutions. Absorption and desorption kinetics have been enhanced through surface treatments or through the production of nanocrystalline/ amorphous Mg_2Ni or related alloys (sometimes with inclusion of catalysts).

Various studies aimed to significantly reduce desorption temperatures have not been successful (Sandrock 1999).

Mg_2Cu has a hydrogen storage capacity of 2.6 wt.% (Reilly and Wiswall 1967). Mg_2Cu has an orthorhombic crystal structure (Pearson symbol: oF48, space group: Fddd) with cell parameters; a= 0.52 nm, b= 0.90 nm, c= 1.83 nm (Gingl et al. 1993).

There are two intermetallics in Mg and Cu system; Mg_2Cu and $MgCu_2$. H_2 does not form hydride with $MgCu_2$ under moderate pressure and temperature conditions. Whereas Mg_2Cu reacts with hydrogen via a disproportionation reaction;

$$2Mg_2Cu + 3H_2 \leftrightarrow 3MgH_2 + MgCu_2 \quad (6)$$

Reilly and Wiswall (1967) reported this reaction occurred fairly rapidly at 300 °C and H_2 pressures of ≈21 bar. In Figure 2.5 several pressure-composition isotherms for the Mg_2Cu-H_2 system are seen.

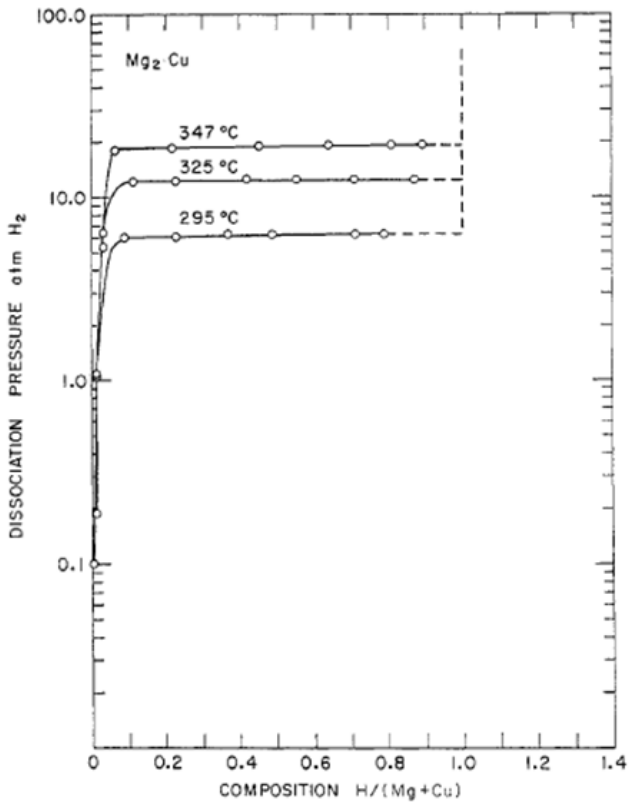

Figure 2.5 Pressure-composition diagram of the Mg_2Cu-H_2 system (Reilly and Wiswall 1967).

Studies dealing with Mg_2Cu are scarce in the literature. In one such study, Jurczyk et al. (2007) investigated thermodynamic and electrochemical properties of nanocrystalline Mg_2Cu-type material. In this study with pure nanocrystalline Mg_2Cu alloy 2.25 wt.% maximum absorption capacity was reached. This value is smaller than that in the conventional Mg_2Cu alloy (2.6 wt.%) due to significant amount of strain, chemical disorder and material defects arisen from the mechanical alloying procedure used. Mechanically alloyed and annealed Mg_2Cu electrode exhibited a maximum discharge capacity of 26.5 $mAhg^{-1}$ at the 1st cycle but this value degraded significantly with cycling due to formation of $Mg(OH)_2$ on the electrodes.

In a similar study, Szajek et al. (2007) studied electrochemical and electronic properties of nanocrystalline Mg_2Cu. They compared discharge capacity of nanocrystalline and microcrystalline alloys at first cycle, when the electrode was charged and discharged at 4 $mAhg^{-1}$. Discharge capacity of nanocrystalline and microscrytalline Mg_2Cu was 26.5, 25.2 $mAhg^{-1}$ respectively.

2.3 Fine Particle Production Methods

There are a number of production techniques to obtain fine particle size such as mechanical milling (Bobet et al. 2000), plasma synthesis (Çakmak et al. 2010), thin film depositions (Westerwaal et al. 2006), spark erosion (Szymczak et al. 2006), electro-deposition (Tsai et al. 2006). Among these, mechanical milling is the most preferable technique to produce hydrogen storage metal hydrides in the form of fine particles. Mechanical milling besides plasma synthesis and thin film deposition techniques are reviewed below.

Mechanical milling (MM) procedure starts with an appropriate powder charge which is generally a blend of elemental powders into a high energy mill, along with an appropriate milling media. The aim of milling is either to refine the particle size or mechanical alloying of particles to obtain a new phase (Yadav et al. 2012) or both.

There are several types of devices for MM. For instance, attritors, planetary mills, horizontal mills and shaker mills are all regularly employed for laboratory and/or large-scale production. However, the basis of powder interaction is essentially the same in all of these devices. Powder particles are broken between colliding balls or between ball and the container walls during MM. These repeated high-energy collisions cause fracturing and cold welding of particles and determine the final structure of the powder, Figure 2.6. Several parameters such as the nature of the milling machine, the ball and bowl materials, the ball to powder weight ratio, the milling atmosphere and process control agents, etc. affect the ultimate microstructure (Huot et al. 2001).

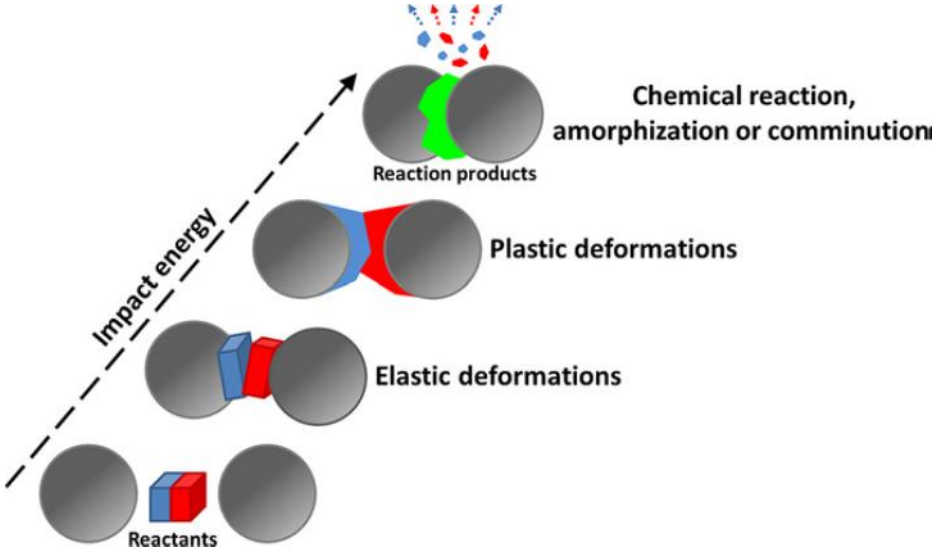

Figure 2.6 Ball collision effects on reactant particles changing with ball impact energy (Huot et al. 2013).

Benjamin and his coworkers (1970) first proposed mechanical alloying (MA) as a method to produce materials by high-energy ball-milling of dissimilar powders for the synthesis of complex oxide dispersion-strengthened alloys. Similar to MM, the typical procedure of MA includes mixing of the powders in the accurate proportion and charging the powder mixture into the mill along with the grinding medium (usually steel balls). This mixture is then milled for the certain length of time until a steady state is achieved when the composition of every powder particle is the same as the concentration of the elements in the initial powder mix. A various studies present that MA and MM could be used to produce amorphous alloys, metastable phases, quasicrystals, extended solid solutions and nanocrystalline materials (Suryanarayana 2001, Huot et al. 2001).

Mechanical milling together with mechanical alloying is the most effective method to synthesize hydrogen storage alloys. The method will be reviewed below with regard to its potential to yield fine particle sizes.

Zaluska et al. (1999) studied the effect of ball-milling on hydrogenation of pure magnesium powder and for this purpose they produced less than 30 nm grain size particles determined by TEM. But SEM images showed that particle size of the produced powder was around 30 μm. They stated that for ball milled powders the improvement of hydrogenation properties arises from primarily the change of microstructure via formation of small grains. They added that the surface modification caused by ball milling such as breaking oxide layers plays a secondary role and this factor also reduces the need for activation.

Liang et al. (1998) investigated the mechanical alloying process of mixed elemental Mg and Ni. Magnesium and nickel powders were mixed and put into hardened steel vial for alloying under purified argon. Sample was stored in a glove-box environment under argon atmosphere to handle it easily. In the as-milled condition, the crystallite sizes of Mg and Mg_2Ni were 20 and 10 nm, respectively.

Jurczyk et al. (2007) synthesized nanocrystalline Mg_2Cu by using mechanical alloying process. SPEX 8000 mill with 30:1 ball-to-powder ratio was used to operate mechanical alloying under an argon atmosphere. According to the Scherrer method, the average crystallite size after 18 h of mechanical alloying was of the order of 30 nm.

Aoyagi et al. (1995) investigated effect of ball milling on hydrogen absorption properties of FeTi. The alloy was produced by arc melting in an argon atmosphere, refined into powder (-115 mesh) using a pestle and a mortar under open atmosphere. Milling procedure was operated using a high energy planetary ball mill. The ball-to-powder ratio of the milling was 13:1. The mean particle size of initial FeTi powder was 45 μm, which was reduced to 16 μm after 86 ks of milling.

Cuevas et al. (2007) determined the hydrogenation properties of $Ti_{0.85}Zr_{0.15}Mn_{1.5}V_{0.5}$ alloy for the microstructure obtained by ball-milling. The alloy was synthesized by arc-melting of the pure elements (minimum purity 99.7%) by using a water cooled-copper crucible under argon atmosphere. Following the alloy was mechanically broken into 1 mm sized particles and put into a stainless-steel vial under argon atmosphere. The alloy was milled in a planetary ball mill with a ball-to-powder ratio of 10:1 at a disc rotation speed of 500 rpm for 20 h. C14 Laves phase with a very strong peak broadening was determined with respect to XRD pattern of the milled alloy. The broadening analysis of this pattern yielded a crystallite size of 3.8 ± 0.2 nm.

The use of hydrides rather than the metals themselves have some advantages. One is that the milled powders which are already hydrided, exhibit better resistance to oxidation than the alloys which have fresh metallic surfaces. This case is valid particularly for magnesium-based alloys. Another advantage is that it is easier to mill hydrides than to mill the elemental metals especially in the case where there is no intermetallic formation (Huot 2001).

Two techniques of direct synthesis of hydrides which are reactive milling and milling elemental hydrides will be mentioned below. In reactive milling, milling procedure is carried out under hydrogen atmosphere. Whereas milling elemental hydrides is carried out under inert atmosphere.

Hydriding properties of a nanostructured composite material of the Mg_2Ni-H system were investigated by Orimo et al. (1997). Up to 1.6 wt.% hydrogen capacity was reached without changing the crystal structure (Mg_2Ni type). They estimated the mean crystallite size of the compound ground for 1 h as 15 nm with respect to TEM observations.

Aoki et al. (1994) pointed out that ball-milling FeTi or Mg_2Ni under argon or hydrogen atmosphere greatly improves the initial absorption rate. Bobet et al. (2000) synthesized Mg and Mg-M (M=Co, Ni and Fe) mixture by reactive milling and also by milling under argon atmosphere. In hydrogen atmosphere, the particle size (initially ≈50 μm) was reduced significantly (≤ 1 μm after 5 h milling). Under the argon atmosphere, the variation of particle size was not remarkable (≈40 μm after 5 h milling). They summarized this difference in a schematic representation shown in Figure 2.7.

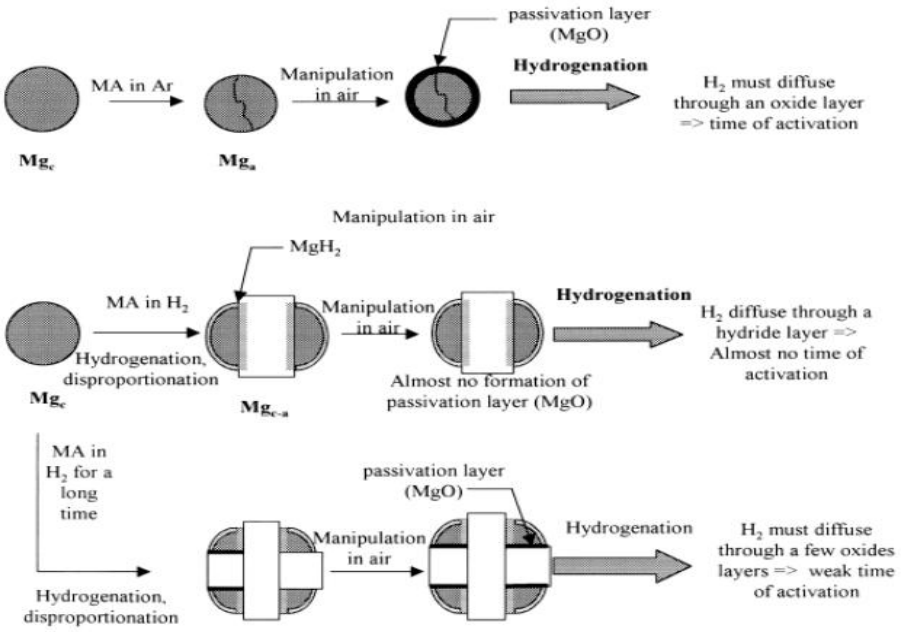

Figure 2.7 Schematic illustration of the reactive and non-reactive milling (Bobet et al. 2000).

When elemental hydrides (or elemental hydrides and basic elements) are milled together in an inert atmosphere, complex hydrides can be produced. Over reactive milling this method has an advantage which is no requirement of special equipment that can keep under control high hydrogen pressures. In addition, especially some hydrides which are difficult to produce, this method may be the solely practical way of production (Huot et al. 2001).
Yavari et al. (2005) examined H-sorption kinetics of MgH_2 powders by using Fe nanoparticles. The two reactants were mixed in desired proportions and milled together for mechanical alloying with ball-to-powder ratio of 200:1 for 72 h under argon atmosphere.

The particle sizes of the composite product determined by TEM observation were mostly within the range of 5–10 nm.

Huot et al. (1999) synthesized Na_3AlH_6 by mechanical alloying. In this study NaH and $NaAlH_4$ powders were mixed with the desired stoichiometry and this mixture was milled in a SPEX 8000 mill with a ball-to-powder ratio of 10:1. Authors did not mention the particle size of the milled powder.

In **thin film deposition,** there is a direct control over the thickness of the deposited layer. This is unlike milling where the nano-size materials are obtained as a result of repeated collisions.

Hydrogen sorption in thin films has been investigated in a variety of systems following the first review of the topic by Wenzl et al. (1983). In such a study Westerwaal et al. (2006) synthesized Mg_2Ni thin films with a thickness of 20, 50 and 150 nm by using vapor deposition. By comparing the surface morphology of samples they proposed an island growth model for the growth of the films. According to this proposal the islands transformed into clusters of fine grains which caused emerging of porous sub-layer with many grains and grain boundaries. Further deposition brought about an increasing grain size which formed a columnar microstructure. This columnar structure existed in the upper side of the film. According to the authors this two-layer microstructure was most probably the reason of the unusual hydrogen uptake in thin films. Westerwaal et al. (2006) observed islands with a grain size of approximately 30, 50 and 100 nm for 20, 50 and 150 nm film thickness, respectively.

Akyıldız et al. (2010) investigated the hydrogenation properties of 300 nm, Pd-capped, Mg–Cu thin films with Cu contents of 5, 10 and 15 at.%. They calculated crystallite sizes for films prepared at 298 K and determined that the crystallite size which was around 50 nm in $Mg_{95}Cu_5$ decreased to a value of 30 nm in $Mg_{85}Cu_{15}$.

As a relatively new technique **thermal plasma synthesis** is, essentially, similar to the thin film deposition. It is appropriate for volume production and from this perspective it can be referred an advantageous technique. In thermal plasma, starting material is vaporized by adequate high temperatures and after that condensed in the quenching zone of the reactor to nano-size scale. Both ceramic and metallic nanopowders are produced by this technique for numerous purposes such as obtaining hydrides of reduced stability (Çakmak et al. 2010).

Suresh et al. (2008) synthesized iron aluminide alloy nanoparticles by DC thermal plasma jet. Iron and aluminum powders which were in the size range between 40 and 100 μm and commercially available were ball milled with an appropriate ratio by weight (Fe-85% and Al-15%) to obtain an iron–aluminum blende. This blende was consumed as feed charge to produce iron aluminide nanoparticles. Obtained nanoparticles had spherical shape and black color. Also they were in the size range between 30 and 70 nm determined by ESEM.

Processing of Mg-10 vol.% Ti powder mixture for hydrogen storage applications was investigated by Çakmak et al. (2010). Plasma processed particle sizes were calculated by BET analysis and determined as in the range of 300-75 nm. These values were approximately three orders of magnitude smaller than those processed with mechanical milling (90-100 μm). For instance Mg particles of 95 μm which were produced by mechanical milling were quite coarse with respect to plasma processed powders where the size was around three orders of magnitude smaller, i.e. 85 nm. In addition the study showed that the crystals derived from plasma processing were relatively defect free, i.e. crystallite size was nearly the same as particle size.

As a consequence, there are several methods to obtain fine particle sizes. These methods are used for various purposes but mechanical milling is the most common and traditional technique to produce hydrogen storage alloy. In this study we propose the decrepitation phenomenon as alternative technique instead of the traditional mechanical milling process.

2.3.1 Measurement of Particle Size

Several methods can be used to measure the particles size; sieving, sedimentation, microscopical measurements, laser diffraction and gas adsorption generally evaluated by BET model. In this section laser diffraction technique and BET analysis will be reviewed.

According to Merkus (2009) only for spheres, the particle size determination with a single parameter (e.g. diameter) is possible. In order to describe a particle of any other shape more parameters are needed. There are various descriptions such as length and width which are directly observed visually and by microscopical techniques. The description can be also based on the concept of equivalent sphere, providing the diameter of a sphere which exhibits the same properties as the particle analyzed. Determination of particle size for different properties may cause different results for the same group of non-spherical particles. For instance sieve diameter, Stokes' diameter and volume diameter are different equivalent sphere diameters.

Particles in a powder material generally are in a distribution of sizes instead of having the same size. In this case, different quantitative descriptors are possible. One possibility is a size distribution comprising number, volume or mass of particles. Other descriptions are a mean size, a single or a small number of data in the middle or at either edge of the distribution or parameters of a model-distribution. For particle size and size distribution, descriptors should be chosen such that best discrimination of the powder product is obtained with regards to desired properties for the analysis of a production process (Merkus 2009).

Current practice is such that **the laser diffraction technique** is used extensively for particle size measurement both in industry and research. The phenomenon behind this technique is that light passing through a suspension is diffracted by a particle with angle which is

inversely proportional to the particle size. The main parts of a typical laser diffraction device are a laser source of coherent light of known fixed wavelength (typically 0.63 μm), an appropriate detector (generally a slice of photosensitive silicon with a number of separate detectors), and a medium containing sample of particles which the laser beam passes through (both liquids and gases mediums are possible for suspending particles). Early instruments used the Fraunhofer theory to derive particle size from diffraction angle but this method can cause large errors under some conditions (for example in the case when the refractive indices of particle material and suspending medium are close each other). Modern instruments are based on the Mie theory to convert interaction of light with matter to particle size. If the refractive indices of the particle material and suspending medium are known, particle sizing in the range 0.1-2000 μm is possible by modern instruments (Rhodes 2013).

Particle size measurements by laser diffraction technique are not always reliable, especially at fine particle sizes. Thus **Brunauer-Emmett-Teller (BET) analysis** is sometimes used to measure the particle size more effectively than laser diffraction technique. This analysis is actually a method for surface area and pore size determination of a powder sample.

BET analysis was first proposed in 1938, Brunauer, Emmet, and Teller. This method is based on a multilayer adsorption model based on Langmuir's kinetic theory. The BET theory states that there is a dynamic equilibrium between uppermost molecules in adsorbed stacks and the vapor. This expresses that where the adsorbate covers the surface in the form if only one layer, there is equilibrium between that layer and the vapor, and where two layers are adsorbed; there is the same equilibrium between the upper layer and the vapor, and so on. Because the equilibrium is dynamic, number of layers covering the actual location of the surface sites may be different but the number of molecules in each layer does not change. As a result the advantage of the BET model is that although exactly one monomolecular layer is never condensed on an adsorbent, it presents an experimental estimation of the number of molecules needed to form a monolayer (Lowell and Shields 1991).

Measurement of adsorbed nitrogen surface area is the most extensive technique for BET analysis. For this purpose single point or multipoint BET methods are used. If the area of the nitrogen molecule is known, an approximation of the total surface area of the sample can be calculated. Before the surface area is calculated, removal of any material which may already be found on the surface is a requirement. This removal procedure is generally carried out by heating under vacuum. It is important because in the absence of it there may be some problems such as limited access of nitrogen to the surface. Single point BET is a standard test method which is used to determine the surface area derived from a single partial pressure whereas multipoint BET results are derived from several partial pressures. The time needed to operate a single point test is less than that of multipoint but can be less proper because of the effect of the surface characteristics. However, the producer or the costumer can choose single point test if high quality measurement is not a must because the handling of equipment and the test is easier (Dick 2003).

In the literature there are several studies which both laser diffraction and BET analysis were used to measure the particle size. In such a study, Wei et al. (2012) analyzed the particle size distribution of magnetite nanoparticles produced by precipitation. For determination of agglomerate size distribution after each experiment suspension samples were taken and diluted to do analysis with laser diffraction granulometer. The average size was found to be 10 μm. The same powder when evaluated with BET analysis was in nanometer range, namely 6-24 nm.

Jiqiao and Baiyun (2001) studied particle size distribution of ultrafine tungsten powder. Table 2.2 is taken from this study where the measurements obtained by laser diffraction and BET analysis are shown. Here the result of BET analysis was converted into an equivalent particle diameter with the use of equation (7).

$$d_{BET} = 6/(S_{BET}.d) \quad (7)$$

Here d_{BET} is the calculated particle diameter, S_{BET} is the specific surface area of the powder obtained by BET analysis and d is the density of the material. This conversion assumes that the particles are spherical in shape.

Table 2.2 Mean particle sizes of tungsten powders evaluated by laser diffraction method and calculated particle diameters via BET analysis (Jiqiao and Baiyun 2001).

Powder status	**Laser diffraction method-mean size (μm)**	**S_{BET} (m^2/g)**	**d_{BET} (μm)**
As-supplied	16.59	5.46	0.057
Lab-milled 1 h	0.85	5.24	0.059
Lab-milled 2 h	0.39	5.16	0.060
Lab-milled 4 h	0.30	4.72	0.066

According to Jiqiao and Baiyun (2001) in laser diffraction method strong ultrasonic dispersion and the appropriate dispersion media could disperse the coarse and loosely formed agglomerates, but due to the existence of severe intergranular and interparticular forces there was almost no way to disperse the rigid and small agglomerates into very fine powders. Hence the results of laser diffraction analysis though reasonable in most cases, may include misleading and incorrect average particle size values and distributions.

When Table 2.2 is examined, it is realized that there is a huge difference between laser diffraction and BET analysis results. This difference which is more than 10 times proves that

laser diffraction and BET analysis do not always conform to each other. Thus with respect to the material studied, appropriate technique should be chosen for more accurate results.

Koley et al. (2011) examined nano-crystalline 2Y-TZP-Al_2O_3 composites. The calcined and ground powders were examined by laser diffraction, BET analysis and X-ray line broadening. Authors have used the term agglomerate rather than the particle and with the laser technique reported a mean agglomerate size in the order of ≈1.5 μm. This value was much larger than the aggregate size (18–45 nm) obtained by BET analysis. The expected nature of particle is seen in Figure 2.8. The crystallite size determined by X-ray line broadening was 8–23 nm. The difference between the laser technique and the BET was explained on the basis of agglomeration which occurs during the measurement. The powder particles in the laser technique need an aqueous suspension/dispersion medium and the surface tension of water gives rise to form agglomerates/flocs easily. As a result, agglomerate size instead of the correct particle size is measured inevitably by the laser diffraction method.

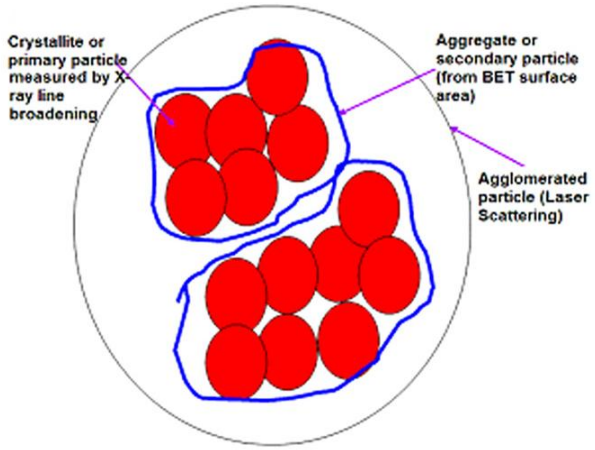

Figure 2.8 Possible natures of particles which reveal the difference between different techniques (Koley et al. 2011).

In conclusion it appears that the laser diffraction technique, in some cases, can yield misleading results. This is especially for particles which have a risk of agglomeration. Because this technique generally requires liquid media such as water, ethanol etc. for suspension purposes, the particles can agglomerate easily in this media. It appears that the use of ultrasonic and stirring equipment can prevent agglomeration in most cases, but when the agglomerate is small and made up of small particles dispersion is difficult to achieve by these equipment. It should be pointed out that the use excessive ultrasonic treatment

sometimes produces the opposite effect and can be the cause of agglomeration itself. The determination of particle size via BET analysis is not subject to such complications. Since BET analysis makes use of gaseous media rather than liquid media, the measurement with BET may be considered more reliable. Because in gaseous media even the gaps between the adherent particles are covered by gas, effective surface area can be calculated and this quantity can be converted to particle size by using several formulas. Contrary in laser diffraction technique, the gaps between the adherent particles cannot be distinguished by laser beam.

2.3.2 Hydrogen Decrepitation

The conventional powder fabrication processes such as ball milling has disadvantages of low efficiency as well as the risk of contamination from the grinding media. So, it is recognized that a process that would allow fragmentation of bulk alloys into small fragments with less energy would highly be desirable. This could be achieved in certain metals and alloys by exposing them to hydrogen atmosphere.

The metals and compounds which could be decrepitated by hydrogen are those that readily react with hydrogen. These cover hydrogen storage alloys such as AB_5, A_2B, AB_2 compounds together with transition metals such as Ti, Zr, rare earth metals and others. The compounds become brittle after hydrogen absorption and can be easily ground into powders or they may be subjected to several cycles of hydrogenation and dehydrogenation which results in in-situ pulverization of starting powders. Hydrogen decrepitation is caused by a large volume expansion during hydrogenation and shrinkage during dehydrogenation.

The use hydrogen processing of rare-earth-based magnets has been examined in Birmingham University since 1978. The earliest study (Harris et al. 1979) was mainly dealt with the hydrogen decrepitation of the intermetallic $SmCo_5$ where decrepitation processed powders were used to obtain a good quality sintered or polymer-bonded magnets (McGuiness et al. 1986). The follow-up studies by the same group has concerned with other permanent magnets; modified Sm-Co (Kianvash et al. 1985) and Nd-Fe-B (McGuiness et al. 1986, Harris et al. 1985).

Hydrogen decrepitation (HD) within the context of hydrogen storage alloys was first reported by Uchida et al. (1984), which simply involves the hydride formation followed by transformation to the initial state. In Mg_2Ni for example when exposed to hydrogen (11.6 bar, 300 °C), forms its hydride namely Mg_2NiH_4 (Sakintuna et al. 2007). Under certain conditions Mg_2NiH_4 transforms back to the original alloy Mg_2Ni. In the case of Nd-Fe-B magnet, hydrogen processing can be more complex; when hydrogenated the compound decomposes into several phases as Nd hydride, Fe_2B and Fe after a heating procedure. Following this when dehydrogenated the phases are combined together forming a single phase $Nd_2Fe_{14}B$. According to Luo et al. (2011) Takeshita and Nakayama (1989) using this treatment opened the way to obtain a very high coercivity levels in Nd-Fe-B magnet. Harris

and co-workers (1991) designated this as HDDR which stands for hydrogenation-decomposition–desorption–recombination processes.

According to Takeshita (1995) in HD processing, hydrogen decrepitation arises from a large volume expansion of the metal lattice when metallic compounds which can absorb hydrogen form solid solutions and/or hydrides. The volume expansions of some intermetallic compounds taken from Takeshita (1995) are re-arranged in the order of increasing volume expansion and are shown in Table 2.3.

Table 2.3 Volume expansions of some intermetallic compounds (Takeshita 1995).

Compound	**Volume expansion (%)**
$Sm_2Fe_{17}H_5$	3.4
$Nd_2Fe_{14}BH_{4.9}$	5.4
$PrCo_5H_{2.8}$	8.2
$SmCo_5H_{2.5}$	7.4
$Nd_2Fe_{14}BH_{2.7}$	4.8
$PdH_{0.706}$	10.4
$TiFeH_{1.04}$	10.5
$LaCo_5H_{3.4}$	10.6
$NdCo_5H_{2.7}$	7.9
TiH_2	15.2
$SmFe_3H_4$	19.0
NdH_3	16.4
$LaCo_5H_{4.2}$	12.9
ZrH_2	18.4
PrH_3	19.3
LaH_3	17.6
$TiFeH_{1.95}$	18.8
CeH_3	21.6
$LaNi_5H_6$	27.3

According to Semboshi et al. (2001) in HD processing, decrepitation is explained in the following manner. When hydrogen is introduced in the surface, this results in the straining due to volume expansion. When the strain exceeds a critical threshold for cracking, spalling occurs in the surface. Fresh surfaces formed by the spalling cause rapid hydrogen absorption which again results in straining. This process continues, thereby leading to pulverization of the starting material. A schematic presentation of this process taken from Graetz and Reilly (2005) is given in Figure 2.9.

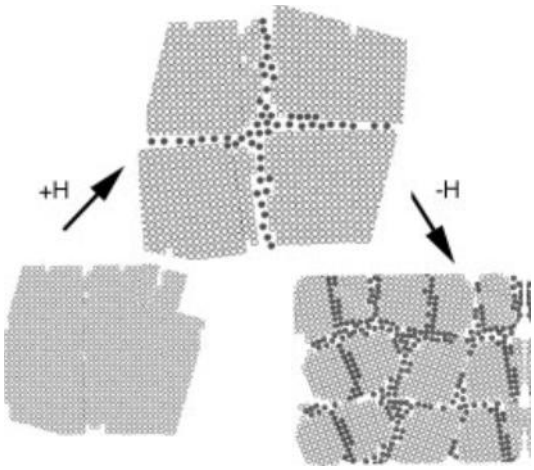

Figure 2.9 Schematic presentation of hydrogen decrepitation process (Graetz and Reilly 2005).

Decrepitation processing has been applied to a variety of materials. These will be reviewed below in the sequence of magnets, hydrogen storage alloys and refractory alloys.

Magnets can be synthesized by a number of different methods including powders, melt-spun ribbons or ingots. Powders can be obtained by mechanical crushing, co-reduction, gas atomization, or HD (Eliaz et al. 2000).

According to Eliaz et al. (2000) the use of the HD process has many advantages for the processing of sintered Nd-Fe-B type magnets. Finer powder and, thus, finer grain sizes are obtained via HD process without excessive oxygen interaction. Through these properties the HD magnets have greater mechanical strength than the standard (i.e. mechanical crushed) products. Some advantages of the HD process are; i) easiness of breaking up the ingot by conventional means because of the presence of free iron, ii) intergranular failure should ensure the synthesis of single-crystal particles, iii) dehydrogenation of green compacts during heating provides a non-oxidizing environment, iv) nearly zero remanent magnetism of aligned green compacts causes easier to handle them, v) it usually allows control of the particles size, shape and distribution by starting manipulation of the microstructure of the alloy and by control of the HD parameters and vi) for subsequent sintering, the very clean surfaces are ideal.

Another related method for the processing of magnets is called HDDR as mentioned above. In Figure 2.10 hydrogen sintering path is superimposed on $Nd_2Fe_{14}B$-hydrogen phase diagram taken from Takeshita (1995). This phenomenon is explained as follows. When the coarse grained $Nd_2Fe_{14}B$ intermetallic compound is heated to approximately 300 °C under a

certain pressure of hydrogen gas (around 1 atm), it first absorbs hydrogen to form $Nd_2Fe_{14}BH_x$. Then, when $Nd_2Fe_{14}BH_x$ is heated under hydrogen to 750–900 °C for 2–3 h, it decomposes into NdH_y hydride, Fe_2B and Fe. Following this, while the material is held under vacuum at the same temperature for 1 h, the NdH_y hydride desorbs hydrogen and recombines with Fe_2B and Fe to form the initial $Nd_2Fe_{14}B$ intermetallic compound. At last, the compound is cooled to room temperature. The desorption and recombination stages are usually applied under vacuum, to obtain unique microstructures consisting of very fine crystalline grains (Eliaz 2000).

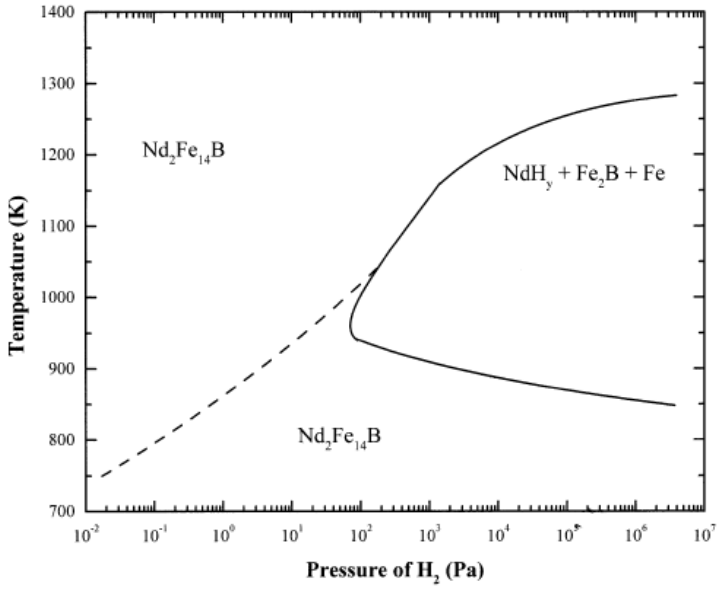

Figure 2.10 Hydrogen–$Nd_2Fe_{14}B$ phase diagram (Takeshita 1995).

Hydrogen processing can be used to synthesize stronger magnets. However, another application of hydrogen processing is in the recycling of magnets. According to Zakotnik (2006) used magnets such as $SmCo_5$, $Sm_2(Co,FeCu,Zr)_{17}$ and Nd-Fe-B can be converted to a powder form because of the expansion of the magnet on hydrogen absorption. Hence recovering of the hard magnetic powder from devices such as hard disk drive or electric motor should be possible by simply exposing the entire system to a hydrogen atmosphere in a specially produced chamber. In this way the exposure of $SmCo_5$ and $Nd_2Fe_{14}B$ to air is avoided as these powders are known to be very reactive. A major advantage of employment of the hydrogen processing is that a further build-up of the oxygen content in the powder during magnet recycling is avoided.

For improved performance in **hydrogen storage alloys** it is necessary to use the material in pulverized form. Decrepitation processing within the context of hydrogen storage alloys has first been reported by Uchida et al. (1984). It must be emphasized that the most hydrogen storage alloys require an initial activation treatment. This treatment may be considered as synonyms to decrepitation. Decrepitation processing will be reviewed below for different classes of hydrogen storage alloys.

Typical **AB_5** compounds used for hydrogen storage purposes cover alloys such as $LaNi_5$, $CaNi_5$, $MmNi_5$ and many complex compositions which are based on the same formula. Of these $LaNi_5$ could be considered as a prototype which has Haucke phases crystal structure. Upon hydriding it transforms to $LaNi_5H_6$ which has hexagonal crystal structure. Takeshita (1995) reported that the lattice volume expansion after this transformation is 27.3%.

Uchida et al. (1984) designed an automated Sieverts-type apparatus to determine the change in the rate of the hydrogen reaction with $LaNi_5$ and the change in size distribution of the alloy particles as a function of absorption-desorption cycles. They observed that the air-exposed $LaNi_5$ particles pulverized under the lower stresses induced by the repeated change in the volume of the alloy during the hydrogenation-dehydrogenation cycles.

The H_2 desorption rate of $LaNi_5H_6$ hydride was examined as with respect to the size of $LaNi_5$ particles and the number (N) of cyclic hydriding and dehydriding reactions by Suzuki et al. (2002). With increasing N, the average particle size diminished from 18 μm at N=10 to 13 μm at N=30, down to 10 μm at N=100.

Hydrogen decrepitation of a low-cost cobalt-free $Mm(Al–Mn–Fe–Ni–Cu)_{5+x}$ alloys were investigated by Yasuda (1997). The alloys were produced using induction melting and thermally treated at temperatures between 1153 and 1353 K in vacuo. The alloy powders were subjected to two consecutive treatments. In the first treatment 32-63 μm alloy powders were exposed to 4 MPa hydrogen at 573 K for 0.5 h and the system was allowed to reach room temperature. The process was applied 3 times aimed for the activation. In the second treatment the system were exposed to 3 MPa hydrogen for 0.5 h and following this evacuated to about 10 Pa for 0.5 h at 313 K. This absorption-desorption procedure was repeated 10 times. The decrepitation behavior as observed in cyclic hydrogenation-dehydrogenation tests is plotted in Figure 2.11. Here decrepitation measured in terms of a factor D which refers to the ratio of mean particle size and after and before cycling, plotted as a function of the initial annealing temperature. It is seen that the most effective decrepitation occurs in alloy A which had been pre-annealed at temperatures less than 1250 K.

Cocciantelli et al. (1997) studied $MmNi_5$ hydrogen storage alloy where elements were partially substituted with Mn, Al and Co ($MmNi_{4.3-x}Mn_{0.33}Al_{0.4}Co_x$). Here the aim of the study was to determine a long term stability of the negative electrode materials to be used in Ni/MH prismatic sealed cells. Alloys were mechanically ground into particles of 45 μm

average diameter. Then pressure-composition isotherms were determined at 60 °C by a Sievert type apparatus. Analysis showed higher decrepitation for low Co content where the average particle size was 20 μm, 15 μm, and 5 μm after 400 cycles for x=0.72, 0.51 and 0.38 respectively.

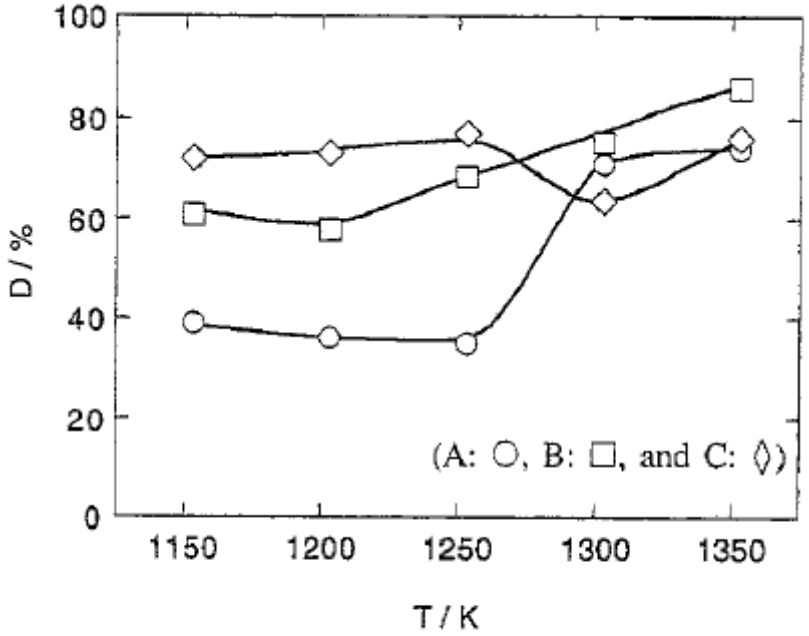

	Composition
A	$MmAl_{0.3}Mn_{0.4}Fe_{0.38}Cu_{0.02}Ni_{3.9}$
B	$MmAl_{0.3}Mn_{0.4}Fe_{0.38}Cu_{0.22}Ni_{3.9}$
C	$MmAl_{0.3}Mn_{0.4}Fe_{0.38}Cu_{0.42}Ni_{3.9}$

Figure 2.11 Decrepitation behavior (D) of the $Mm(Al–Mn–Fe–Ni–Cu)_{5+x}$ alloys treated at different temperatures (Yasuda 1997).

In literature it is quite common to investigate the changes in crystallite size during processing or the use of hydrogen storage alloys. In one such study, Alcantara et al. (2001) studied the effects of decrepitation and corrosion on AB_5 type $MmAl_{0.2}Ni_{3.97}$ $Co_{0.41}Mn_{0.64}$ alloy used in Ni/MH batteries. The study using X-ray diffraction yielded average crystallite sizes of 815 Å and 336 Å before and after 30 electrochemical hydrogenation cycles respectively.

Shan et al. (2011) developed thin-film inks based on $LaNi_{4.7}Al_{0.3}$ and $CaNi_5$ to be used as a hydrogen storage module for onboard electrical power source appropriate for micro-electro-mechanical systems (MEMS). A schedule was used which involved 10 min absorption under approximately 110 kPa hydrogen and 10 min desorption in vacuum. The schedule was repeated for as many as 5000 cycles. Before the schedule, the particle size of $LaNi_{4.7}Al_{0.3}$ was less than 15 μm, and after 5000 cycles, the particle size was approximately 2 μm, i.e. the particle size decreased about 8 times. For $CaNi_5$ ink, the particle size was around 50 μm before the test, and after the test, the particle size was approximately 5 μm, i.e. a decrease of about 10 times.

Typical compounds that are **A_2B** type used for hydrogen storage purposes cover alloys such as Mg_2Ni, Mg_2Cu and Ti_2Ni. Of these Mg_2Ni could be considered as a prototype which has hexagonal crystal structure. Upon hydriding it transforms to Mg_2NiH_4 which has monoclinic crystal structure. The lattice volume expansion after the transformation is 32.1%.

Cyclic hydriding/dehydriding reactions in Mg_2Ni alloy was studied by Lin et al. (2011). In this study, the initial powder size 200 mesh (74 μm) decreased to around 1 μm after 50 cycles of hydriding/dehydriding reactions, Figure 2.12.

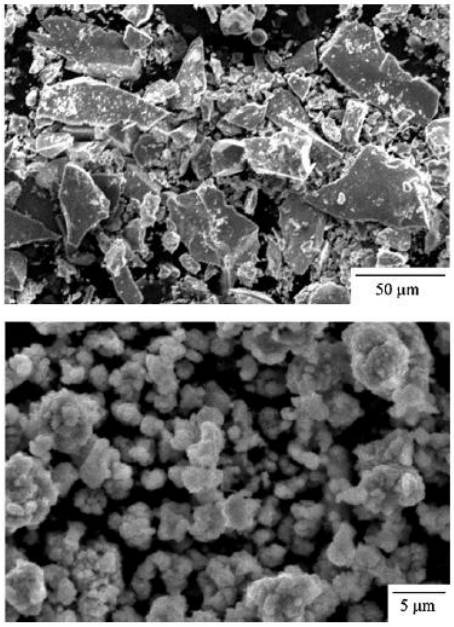

Figure 2.12 SEM images of initial Mg_2Ni powders (above) and after a 50-cycle hydriding/dehydriding test (below) (Lin et al. 2011).

Shan et al. (2006) reported that reduction of the activation pressures is possible via mechanical grinding a small amount of palladium with the hydrogen storage alloys. Also they showed that palladium treatment of Mg_2Ni significantly improved the hydrogen storage performance of that intermetallic alloy. After grinding, the particle sizes were measured by SEM and were around 50 μm or less, with a range of particle sizes. The absorption and desorption rates increase considerably and stabilize at the higher rates after absorption/ desorption cycles. 200 min half reaction time in the first hydrogen absorption diminished to 12 min after 5 cycles.

Typical compounds that are $\mathbf{AB_2}$ type used for hydrogen storage purposes cover alloys such as ZrV_2, $ZrMn_2$ and $TiMn_2$. Of these $ZrMn_2$ could be considered as a prototype which has C14 Laves phase crystal structure. Upon hydriding it transforms to $ZrMn_2H_{3.6}$ which has hexagonal crystal structure. The lattice volume expansion after the transformation is 23.7%.

Arun and Ramaprabhu (1997) examined decrepitation and cyclic stabilities in ZrMnFe alloy with C14 Laves phase structure. The alloy was exposed to only eight cycles (desorption at 250 °C and absorption at 1 bar and at RT). The results pointed out that there was a drastic increase in the number of particles in the lower size range after just eight hydrogenation cycles. Figure 2.13 is taken from this study which shows histograms of particle size distribution with cycling. At the same time much softer alloy $Zr_{0.2}Tb_{0.8}Co_3$ was investigated as well. Even after thirty-five cycles of hydrogenation, there was very little change in the particle size of this alloy.

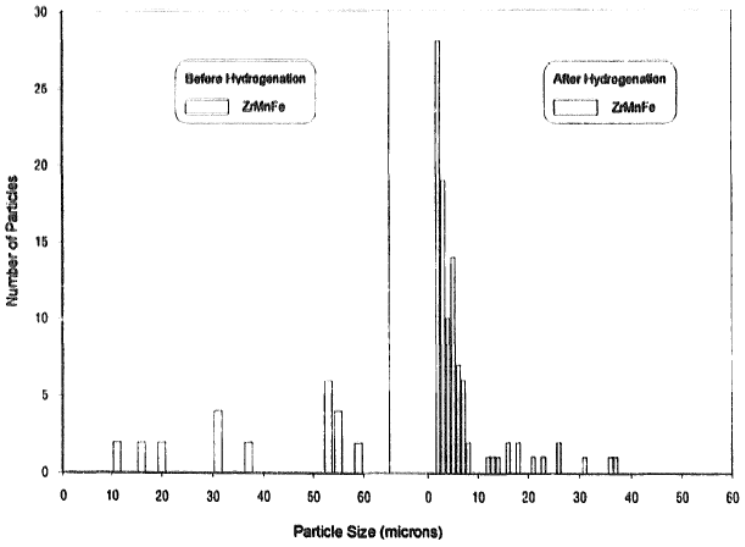

Figure 2.13 Particle size distributions in ZrMnFe alloy (Arun and Ramaprabhu 1997).

As mentioned in section 2.2 Ti-based alloys of AB_2 type alloys are multiphase alloys formed by BCC and Laves phases (Hirscher 2010). Yu et al. (2004) investigated the effect of Cr content on hydrogen storage properties for Ti-V-based BCC-phase alloys. They suggested that the activation of C14 Laves phase is easier than BCC phase in the alloy system. They explained as follows: the hardness of BCC-phase alloys are high and are more difficultly pulverized than C14 Laves-phase alloys. In pulverization of alloys with Laves phase, cracking occurs easily resulting to form of new fresh surface. More hydrogen will penetrate into the bulk alloy through the newly formed fresh surface and lattice expansion because of hydrogenation of alloy will increase further cracking. The alloys would be activated easily in this manner. The ratio of BCC phases increases with increasing Cr amount. Thus pulverization of the alloy becomes more difficult, which causes the activation of the alloy more difficult as well.

Miraglia et al. (2012) investigated means of pulverizing $Ti_{1-x}V_{1-y}Cr_{1+x+y}$ ($x \leq 0.4$, $y \leq 0.3$) and Zr_7Ni_{10} hydrogen storage alloys. The authors co-melted the main BCC phase with a minor metallic ingredient so as to be used as activating/pulverizing phase. After melting, synthesized batches of samples were hand-crushed into coarse powders (200 μm) using a steel mortar in air, for further co-melting. In order to determine PCT characteristics each sample was heated up to 150 ºC during 1 h under primary vacuum and then cycled three times at 50 ºC, 1 MPa for absorption and 250 ºC, 2 kPa for desorption. In Figure 2.14 the Gaussian profile of grain size distribution which is in log scale and centered on 50–60 μm determined with the hydrogenated compound is seen.

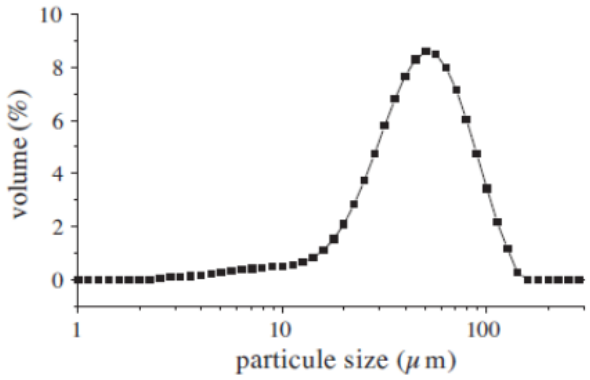

Figure 2.14 Grain size distribution after hydriding of $TiV_{0.8}Cr_{1.2}$ + 4 wt.% Zr_7Ni_{10} (Miraglia et al. 2012).

Semboshi et al. (2001) studied degradation of the hydrogen absorbing capacity in cyclically hydrogenated $TiMn_2$ (Ti–60 at.% Mn) with Laves structure. Ti–60 at.% Mn is composed of Laves phase $TiMn_2$ and a small amount of TiMn. As-cast Ti–60 at.% Mn product was crushed into chips with sizes of about 1000 μm. Hydriding procedure was carried out at room temperature. One hydrogen cycle included pressure increasing to 3.2 MPa and subsequent to pressure reduction to less than 0.01 MPa. The first hydrogenation cycle caused considerable refinement to particle size mostly less than 30 μm. Fractured surfaces appeared to be composed of crystallographic facets. Powder particles which were smaller than 10 μm increased after 30th hydriding cycle. Despite the further improvement of the pulverization via cyclic hydrogenation, the refinement of particle size from 1st to 30th cycle was slow in comparison with the rapid change in the first cycle. SEM micrographs taken from this study are reproduced in Figure 2.15.

Murshidi et al. (2011) studied a C14 Laves phase alloy with composition Ti0.97Zr0.019 V0.439Fe0.097Cr0.045Al0.026Mn1.5. This alloy reversibly stores hydrogen under ambient temperatures. The alloy was first exposed to 50 bar of hydrogen at room temperature for 1 h, and then subjected to an evacuation step. This hydriding/dehydriding activation cycle was repeated 3 times. After completion of the activation procedure, the residual hydrogen within the sample was removed by evacuation at room temperature for 24 h. The pressure-composition isotherm measurements were then carried out at 25, 40 and 60 °C. The mean particle size prior to hydrogen sorption was 50-200 μm. After the sample was hydrogenated multiple times the particle size reached to generally less than 20 μm and the fractured particle surfaces appeared to consist of smooth crystallographic facets.

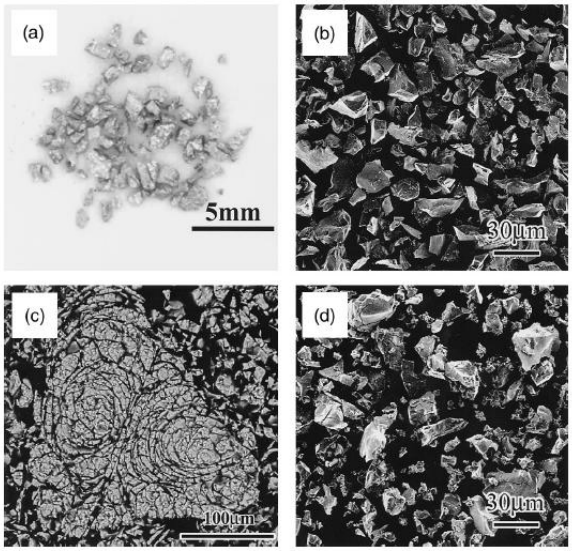

Figure 2.15 SEM micrographs of Ti–60 at.% Mn alloys; a) before hydrogenation, b) after 1st cycle, c) cross-section view after 1st cycle and d) after 30th cycle (Semboshi et al. 2001).

Hydrogen decrepitation is also applied to **refractory alloys**. Hydrogen-induced fragmentation behavior of Ta–Ni binary alloys was examined to determine the mechanism of hydrogen pulverization of refractory metals and alloys by Semboshi et al. (2003). In their study, sample shape of single-phase alloy of Ta solid solution did not change via hydrogenation at room temperature, whereas two-phase alloys of Ta solid solution and Ta_2Ni Laves phase were broken into fragments.

The follow-up study by the same group was carried out for two-phase $NbCr_2$/Nb solid solution refractory alloy (Semboshi et al. 2004). The alloy was pulverized upon a large amount of hydrogen absorption. They proposed that cracking which causes to pulverization is initiated at brittle intermetallic regions or hydrides, which are fractured by lattice expansion of Nb solid solution because of hydrogen absorption.

As a consequence according to Semboshi et al. (2003) general features to obtain a substantial size reduction in hydrogen processing are as follows; i) alloy should compose of two phases, ii) at least one phase should absorb hydrogen greatly, form hydride and iii) at least one phase should be a brittle intermetallic. They further mentions that i) pulverization starts at sample surface and progresses to form delamination from surface, ii) shape of fragments is flake-like and iii) crack spreads preferentially through a brittle phase.

According to Takeshita (1995) intermetallic compounds decrepitate into finer powers after less lattice expansion than elemental metals, whereas elemental metals tend to keep their integrity even if their lattices are expanded to a large extent. Takeshita (1995) attributed this difference in elemental metals and intermetallic compounds to lattice elasticity, because elemental metals are softer than intermetallic compounds. Takeshita (1995) further points out that in decrepitation of polycrystalline materials there are two modes of disintegration; intergranular and intragranular. It is obvious that the intragranular or intergranular breakage will occur whenever the volume expansion caused by hydrogen absorption is large enough for decrepitation. In the absence of enough volume expansion intragranular breakage will not be observed. In such cases intergranular disintegration may or may not occur depending on the existence of boundary phase(s) and the hydriding characteristic.

CHAPTER 3

EXPERIMENTAL PROCEDURE

3.1 Materials

Two alloys were prepared within the context of this research; Mg_2Ni and Mg_2Cu. Starting materials Mg was obtained in powder form Alfa Aeser, 99.8 % and 325 mesh as well as in the form of cast block from Aveks (99.9 % purity). Similarly nickel powder was obtained from Alfa Aesar, 99.9% and - 300 mesh. Copper used was electrolytic grade in the form of a rod 10 mm in diameter.

3.2 Vacuum/Pressure Induction Melting

Alloys were prepared using a vacuum/pressure induction melting furnace (Linn High Therm MFG 30/5-150), Figure 3.1. This furnace is made up of four parts; the vacuum/pressure melting chamber, induction generator, chiller and the control unit. The chamber was in the form of a cylinder with approx. 775 mm in diameter and 775 mm in depth. It was designed to withstand a pressure of 10 bar. The chamber had a lid which could be closed using 32 bolts symmetrically placed at its periphery. An O-ring with an elliptical cross section was used to make the chamber vacuum/pressure tight. The chamber had three large diameter flanges connected to it. The top flange incorporated a viewport whereby the temperature of the furnace could be monitored via a pyrometer. Induction generator was of a medium frequency type with 30 kW power.

The furnace could be operated using induction coils designed to accommodate ceramic crucibles with or without graphite inserts i.e. melting could be carried out within the ceramic crucible or within the graphite crucible within it. Melting could also be carried out using a cold crucible, for which it was necessary to change the induction coil. The cold crucible had a conical shape with 10 fingers with a diameter of 45 mm (diameter at the bottom was 25 mm) and the height of 60 mm Figure 3.2.

The operating procedure for the furnace was as follows. Having closed the lid, the chamber was taken under vacuum (typically 10^{-2} mbar). Then the chamber was flushed with argon (99.995% pure) to typically 700 mbar. This was repeated three times and at the end of the third cycle the pressure was increased to approximately 8 bar. The furnace was then considered ready for melting.

Figure 3.1 The view of vacuum induction melting system.

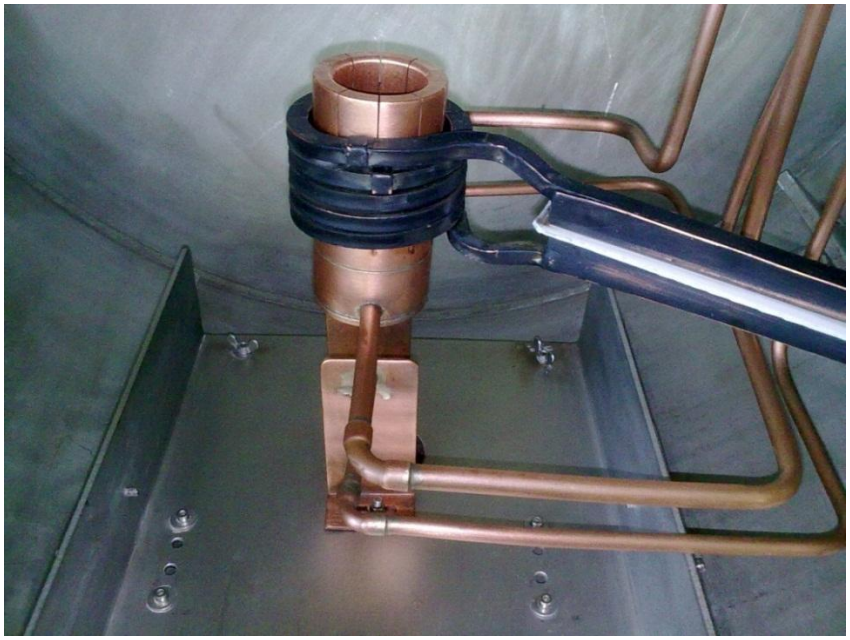

Figure 3.2 The photograph of cold crucible.

3.3 Alloy Preparation

The alloys prepared in this study were Mg_2Ni and Mg_2Cu. Since both alloys have a substantial amount of Mg it was necessary to carry out the melting under pressure.

Mg_2Ni was melted with cold-crucible. Since the pyrometer of the furnace operates starting from 900 °C, this was of little use for the current alloys where Mg already melts at 650 °C. The use of temperatures higher than normal leads to Mg evaporation despite the applied pressure. Therefore two preliminary experiments were carried out for further studies in order to determine the best melting practice for efficient power coupling in cold crucible melting.

These preliminary experiments were carried out with steel. For the first experiment a total of 5 cylindrical steels were prepared where the height of the samples varied in the range 10, 20, 27, 30 and 40 mm, the diameter being kept constant 30 mm. In order to melt these samples, the furnace was operated with full power. Samples with height of 10 mm could not be melted. Thus a minimum height of 20 mm was required for successful melting. Difficulty in melting was attributed to misalignment of crucible with respect to induction coil. In cold crucible the standard practice is to align the crucible such that one turning of the coil is below the bottom of the crucible.

In the second experiment, the diameter was changed from 30 mm to 39 mm as the heights of the samples were kept at 45 mm. In this experiment the same heating procedure was applied to all samples and power coupling values and melting processes were monitored. Applied powers versus coupling curves as well as the temperatures versus applied powers are given in Figure 3.3. It is seen that temperatures reached for the same applied power generally increases with increased diameter of the samples. Differences, however, were not great and samples diameter $\geq$ 30 or 35 mm are considered appropriate for the purpose.

Based on above observations, the size was selected as 30-35 mm diameter and 20-30 mm in height. Accordingly 40 g of stoichiometric powder were prepared by mixing Mg and Ni powder (i.e. Mg–54.7 wt.% Ni). The mixing was carried out in a SPEX mill using a single 15 mm diameter steel ball at ball-to-powder weight ratio of 2:3 for 15 minutes.

Mixed powders were pressed to pellets of 30 mm diameter with a height of 11 mm under a pressure of 250 MPa. Two pellets were placed one above the other and melted under an argon pressure of 8 bar. Following the melting, the alloy was removed from the cold crucible. It was first broken into pieces inside a plastic bag and then hand-crushed in a ceramic mortar.

The alloy **Mg_2Cu** was prepared using graphite crucible. A total of 125 g of alloy was prepared by placing pieces of Mg and Cu cut from the bulk materials in stoichiometric proportions. Melting was carried out under 8 bar argon pressure. Having removed the alloy

from the furnace it was first broken into pieces inside a plastic bag and then hand-crushed using a ceramic mortar.

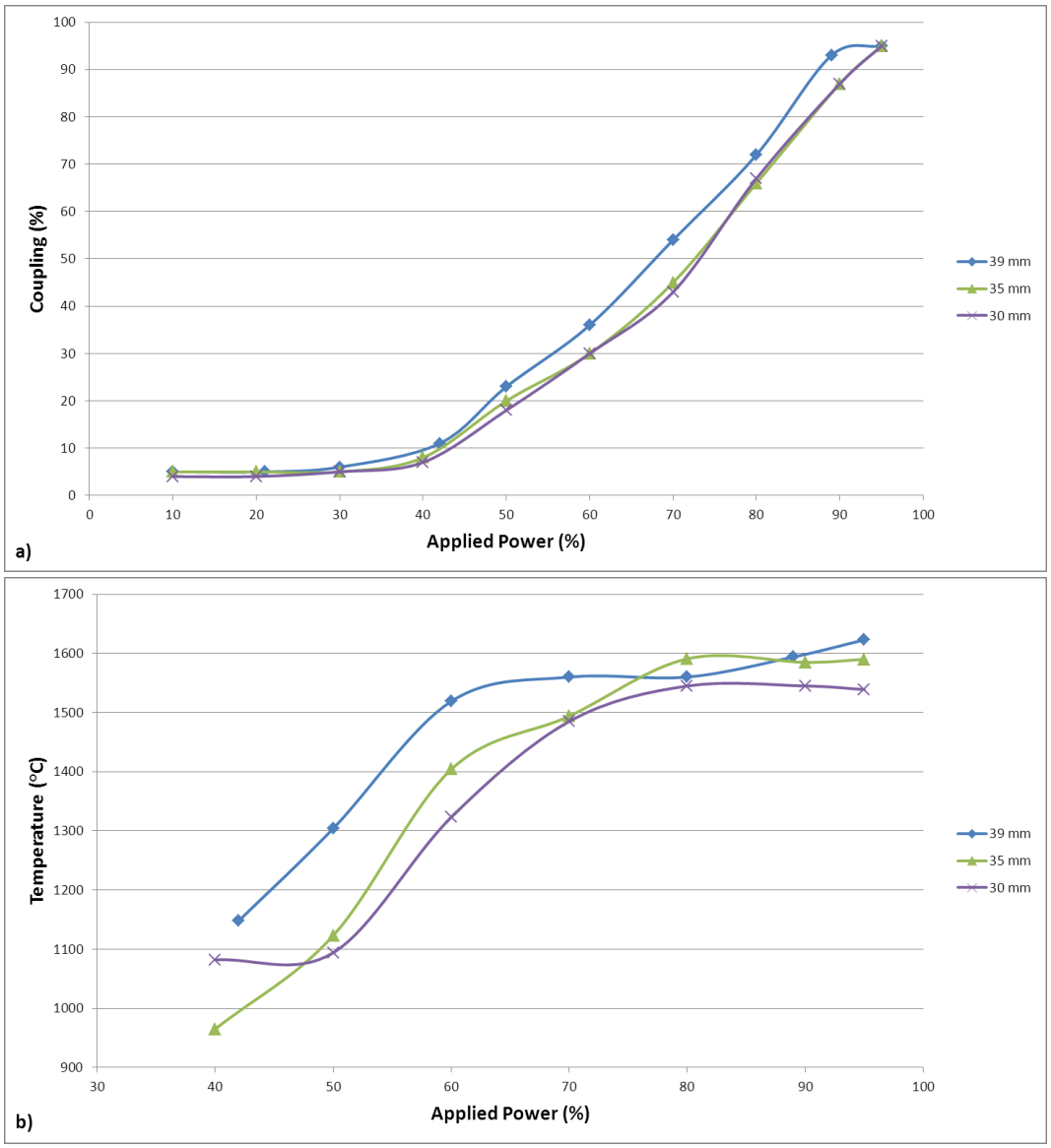

Figure 3.3 Preliminary heating experiments in cold-crucible with steel samples of different diameters (height: 45 mm); a) applied power versus coupling and b) applied power versus temperature reached in the samples.

3.4 Decrepitation Treatment

Decrepitation treatment was carried out in an apparatus originally designed for PCT measurement, i.e. a Sievert type apparatus. This allowed the use of temperatures up to 400 °C and vacuum levels down to 10^{-3} mbar, Figure 3.4. Apparatus was computer controlled whereby the temperature and pressure data could also be recorded.

The treatment starts by placing the sample into a reactor which was then taken under vacuum typically down to 10^{-1} mbar. The reactors used for this purpose is shown in Figure 3.5. The reactor was then flushed with high purity argon (99.998%). Following this procedure, the reactor with 1 bar of argon pressure was heated up to generally 350 °C. Having reached this temperature high pressure hydrogen was released to the reactor.

Figure 3.4 Custom-made apparatus used for decrepitation treatment.

The reactor under hydrogen pressure was allowed to cool down to temperatures generally less than 60 °C. Having reached this temperature the furnace was reactivated and the reactor was heated to the same temperature as before. A total of typically 10 cycles were applied during which temperature and the pressure was monitored and recorded.

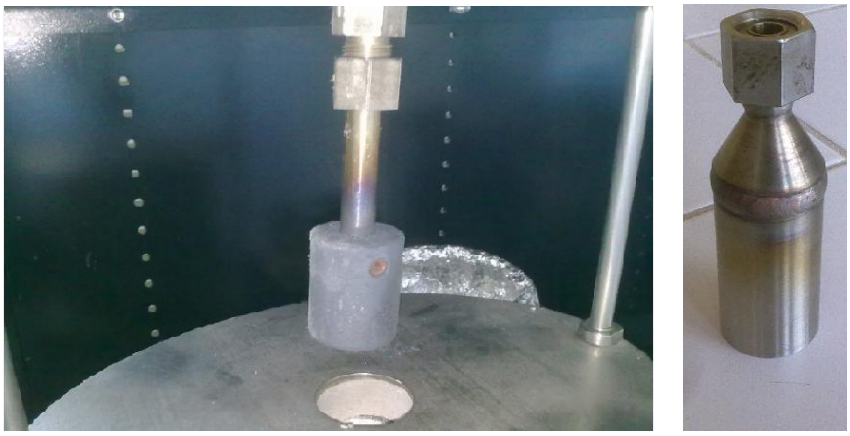

Figure 3.5 The small (left) and the large (right) reactors used for the decrepitation treatment.

Two types of treatment were applied; i) a non-stop and ii) interrupted hydrogenation and dehydrogenation cycles. In the latter, the experiment was interrupted where small samples are removed from the main batch for characterization purposes.

In the non-stop experiment, the typical treatment begun with charging of 1 g alloy powder into the reactor which was then taken under vacuum. Several vacuum-argon cycles were applied to purge the system. With the sample inside the reactor under 1 bar of argon was then heated to 350 °C. Having reached the temperature it was charged with 35 bar of hydrogen. The reactor was then allowed to cool down to room temperature while monitoring the temperature and pressure. A sudden pressure drop during cooling was a sign of hydrogenation. Having reached the room temperature the 1st cycle was terminated.

The second cycle starts with dehydrogenation where the reactor is heated up to 350 °C. A sudden increase in pressure during heating was a sign of a dehydrogenation process. Having reached 350 °C, the heating was stopped and the reactor was then let to cool down in a controlled manner. Having reached room temperature the sample was at the end of 2nd cycle. The process was repeated at least 5 times, i.e. a total of 5 cycles, but in the case of Mg_2Cu, the process was continued to 10 cycles.

In the interrupted experiments 10 g alloy powder was used. The typical experiment was carried out in the same manner as above, except for the fact that having reached the room temperature, the reactor was removed from the system and moved to glove-box. A sample of 1.5 g was removed the main batch and the reactor having been closed returned to the system. The system was taken under vacuum at room temperature and charged with hydrogen and the experiment was continued. Samples were obtained after 1st, 3rd, 5th, 7th and 10th cycles.

3.5 Material Characterization

Samples were characterized by X-ray diffraction (XRD) using Rigaku DMAX 2200 theta/theta diffractometer using Cu-K_α radiation in Bragg-Brentano mode. Structural characterization was carried out using FEI Nova Nano 430 scanning electron microscope (SEM). For powder samples, double sided carbon tape is used to attach powders to the SEM grid.

Particle size measurements were carried out both with laser diffraction and BET analysis. Measurements for laser diffraction were taken with Malvern Mastersizer 2000. Measurements were carried out in ethanol as dispersion media with an ultrasonic treatment of typically 20%.

Brunauer-Emmett-Teller (BET) analysis was carried out in Quantachrome Corporation Autosorb-6. Multipoint method was used to measure the surface areas.

CHAPTER 4

RESULTS AND DISCUSSION

4.1 Hydrogen Decrepitation of Mg_2Ni

40 g of Mg_2Ni alloy was melted under 8 bar of argon pressure using cold-crucible. Backscattered SEM micrograph of as-solidified alloy is given in Figure 4.1. X-ray diffractogram of Mg_2Ni produced and ground to fine powder is given in Figure 4.2. As seen in the figure, the sample has peaks complying with Mg_2Ni (JCPDS card no: 35-1225). The phase has hexagonal crystal structure with lattice parameters of a= 5.21 Å, c= 13.23 Å. In addition a negligible amount of $MgNi_2$ phase (JCPDS card no: 25-1374) was detected in the diffractogram and this case is supported by the contrast difference seen in Figure 4.1.

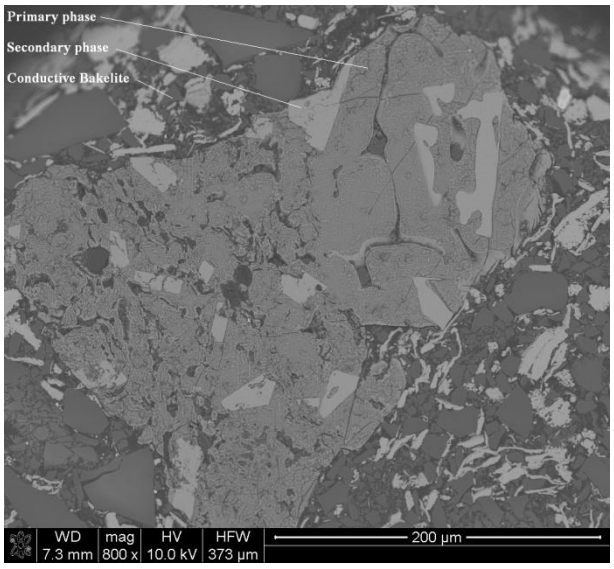

Figure 4.1 SEM micrograph of as-solidified Mg_2Ni (matrix surrounding the particle is conductive Bakelite).

Mg_2Ni was hand-crushed to an average particle size of 100 µm. 1 g of crushed sample was placed in a reactor and was subjected to 5 hydrogenation cycles (see in section 3.4). The cooling and heating rate for (de)hydrogenation was approximately 7 °C/min. Pressure-

temperature curves recorded during the experiment for the sample are given in Figure 4.3. It is seen that both absorption and desorption improved with cycling. The difference between 1st and 2nd cycle was particularly large. In the 1st cycle, the pressure drop from 350 °C to 100 °C was in the order of 3.16 bar, in the 2nd cycle this value has increased to 4.44 bar. After the 5th cycle, the pressure drop had a value of 6.1 bar.

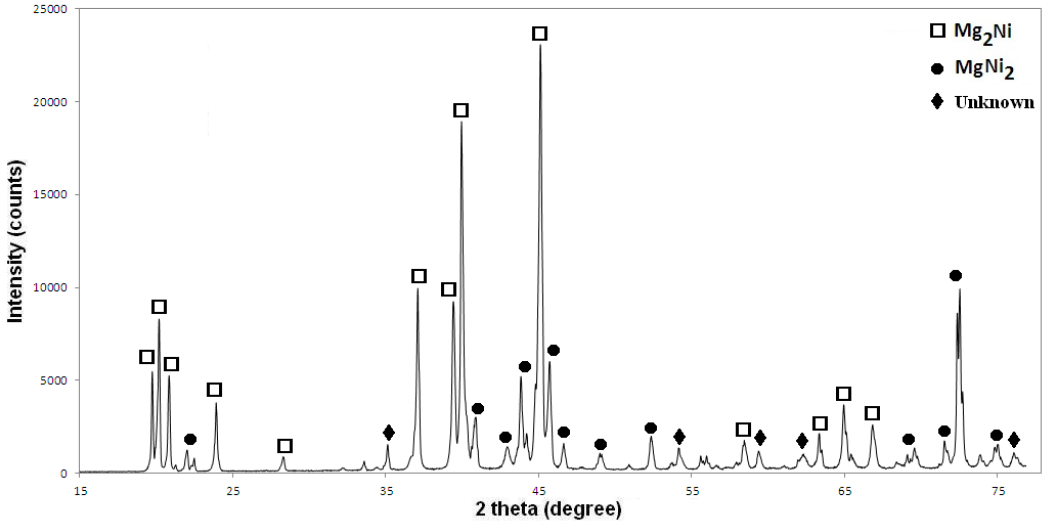

Figure 4.2 X-ray diffractogram of Mg_2Ni produced.

Sample following the 5th cycle was examined with X-ray diffraction. The pattern is given in Figure 4.4 where the sample complies with Mg_2NiH_4 (JCPDS card no: 38-0792, crystal structure: monoclinic, lattice constants: a= 6.496, b= 6.412, c= 13.204).

SEM images of the powder sample before and after the decrepitation treatment are given in Figure 4.5. It is seen that powders were decrepitated as a result of cycling. The appearance of SEM images is such that decrepitated particles are in the form of colonies that seem to have been derived from the starting powders. These colonies are quite large, have a crumbled form and seem to be made up of collection of smaller particles

In order to investigate the process of decrepitation in depth a separate experiment was carried out for 10 hydrogenation cycles. For this purpose 10 g of sample was used and the experiment was interrupted to remove a sample at the appropriate cycles (see in section 3.4). The cooling and heating rates were again 7 °C/min.

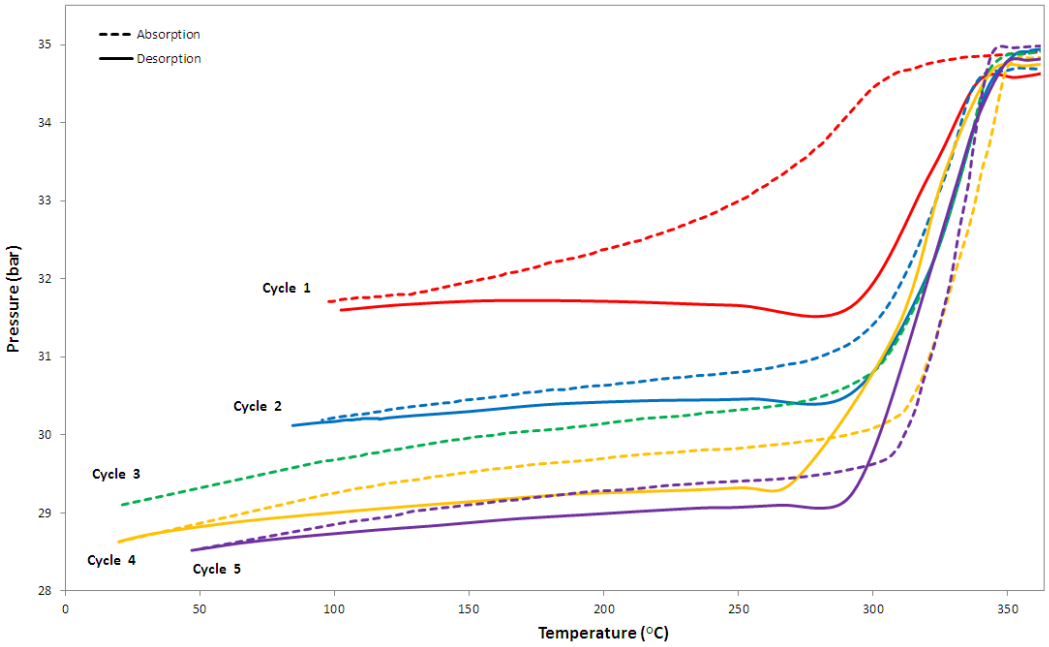

Figure 4.3 Absorption and desorption curves of Mg_2Ni applied 5 cycles.

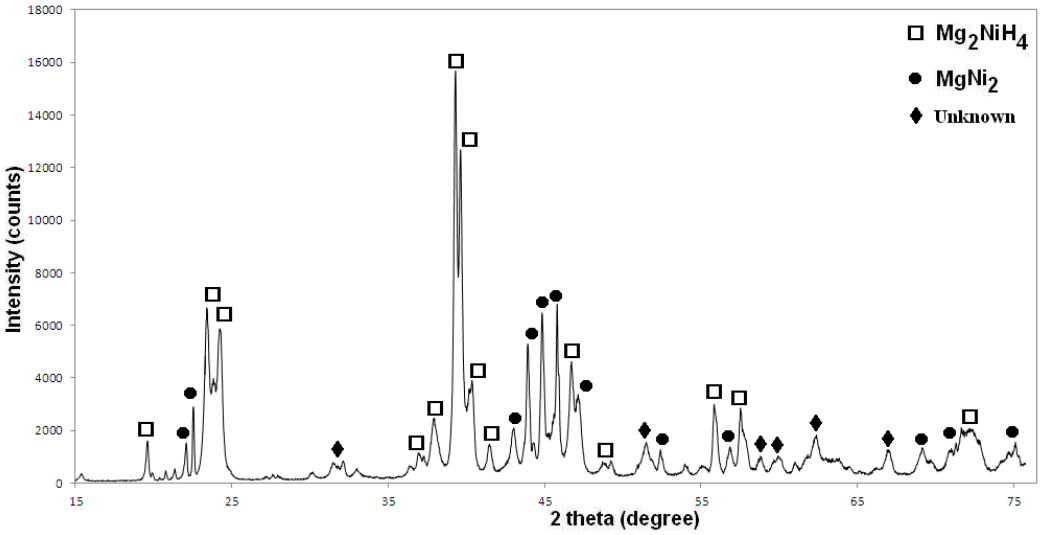

Figure 4.4 XRD diffractogram of Mg_2NiH_4 after the experiment.

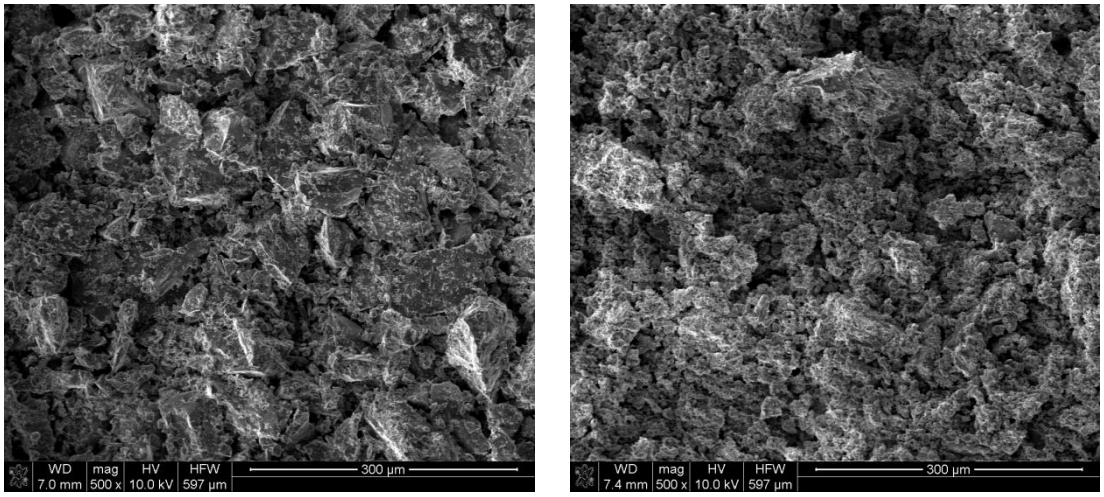

Figure 4.5 SEM images of Mg_2Ni before decrepitation (left) and Mg_2NiH_4 after decrepitation (right).

The samples removed from the reactor were evaluated with respect to particle size. This evaluation was initially carried out with a laser diffraction method. But since measurement of particle size with laser diffraction is not always reliable, samples were also characterized with BET analysis. Assuming that particles are spherical the surface area measured with BET analysis was converted to particle size using equation (8).

$$d_{BET} = 6/(S_{BET}.d) \quad (8)$$

Here d_{BET} is the particle size, S_{BET} is the surface area of the powder and d is the density of the material. Densities of Mg_2Ni and Mg_2NiH4 were taken as 3.43 g/cm^3 (Pasturel et al. 2007) and 2.57 g/cm^3 (Varin et al. 2009), respectively.

Particles sizes measured for the powders as a function of cycling are reported in Table 4.1. Here the values reported are the particle sizes determined with laser diffraction, BET surface area and the particle sizes derived from the BET measurement. Particle sizes calculated by laser diffraction and surface areas determined by BET analysis are also shown plotted in Figure 4.6. It is seen that the particle size decreases with cycling. In terms of values measured by laser diffraction, the minimum particle size reached at the end of 10th cycle is roughly 30 microns. This value probably refers to colonies rather than the actual particle size. Minimum size measured with BET analysis corresponds to a particle size of 700-800 nm. This size is more representative of the microstructure reported in Fig. 4.5.

Table 4.1 Surface areas calculated by BET analysis and particle size values obtained by laser diffraction technique and BET analysis for Mg_2Ni.

Cycle number	Particle size (µm)-laser Diffraction	Surface area (m^2/g)-BET	Particle size –BET (µm)
0	54.1	0.42	4.16
1	48.8	2.13	1.09
3	42.1	2.89	0.8
5	36.7	3.26	0.71
7	-	2.89	0.8
10	32.5	3.07	0.76

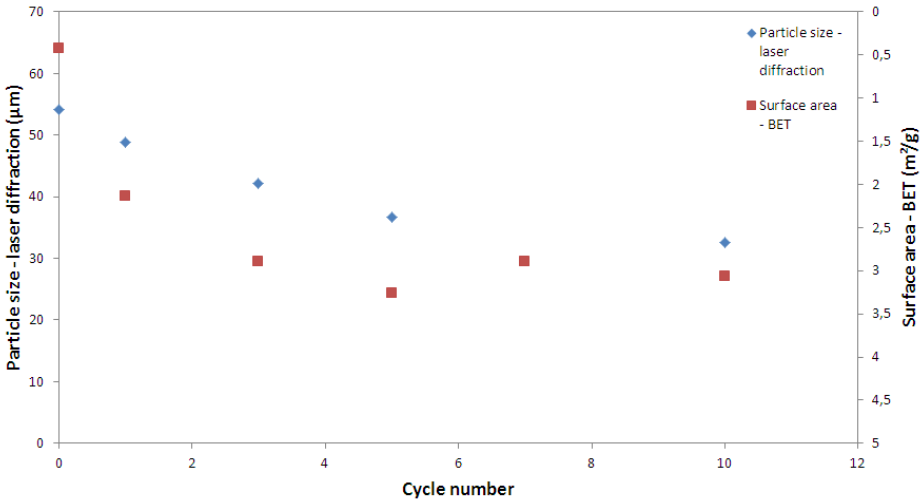

Figure 4.6 Particle sizes measured by laser diffraction and surface areas determined by BET analysis versus cycle number for Mg_2Ni.

Pressure changes recorded during cycling are given in Figure 4.7 in the form of arbitrary units. Here both pressure drop which occurred during absorption and the pressure increase which occurred during desorption are given. It is seen that in the first few cycles the change is quite large but with cycling the magnitude of change is diminished.

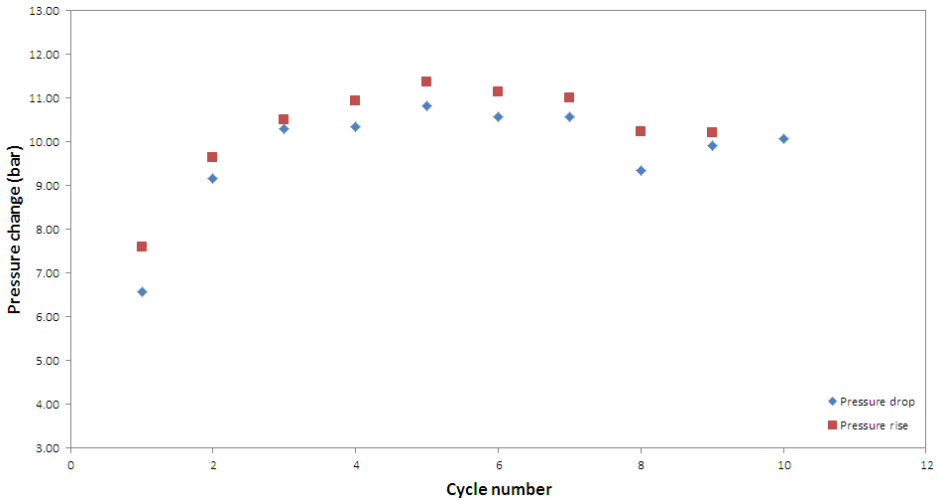

Figure 4.7 Pressure drop at room temperature and pressure rise at 350 °C in Mg_2Ni with cycling.

4.2 Hydrogen Decrepitation of Mg_2Cu

125 g of Mg_2Cu alloy was melted under 8 bar of argon pressure using graphite crucible in an induction furnace. Backscattered SEM micrograph of as-solidified alloy is given in Figure 4.8.

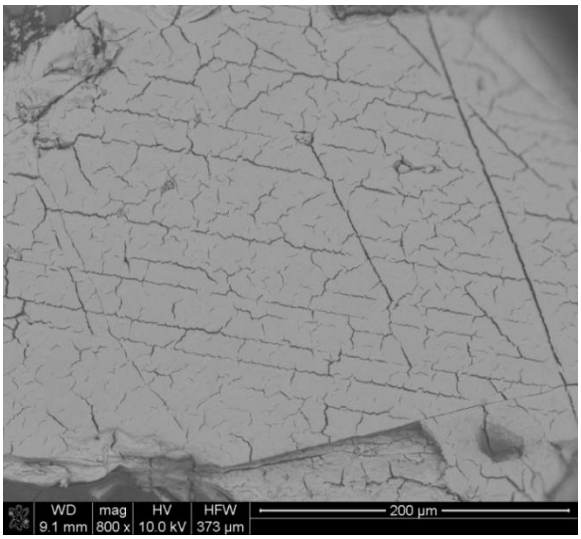

Figure 4.8 Backscattered SEM micrograph of as-solidified and crushed Mg_2Cu alloy.

X-ray diffractogram is given in Figure 4.9 for Mg_2Cu ground to fine powder. The pattern is compatible with Mg_2Cu (JCPDS card no: 65-1116) which has orthorhombic crystal structure with lattice parameters of a=9.044 Å, b= 5.275 Å, and c= 18.328 Å. Rietveld analysis carried on the pattern showed that Mg_2Cu was 97.4 wt.% and the remaining phase was Mg with 2.6 wt.%.

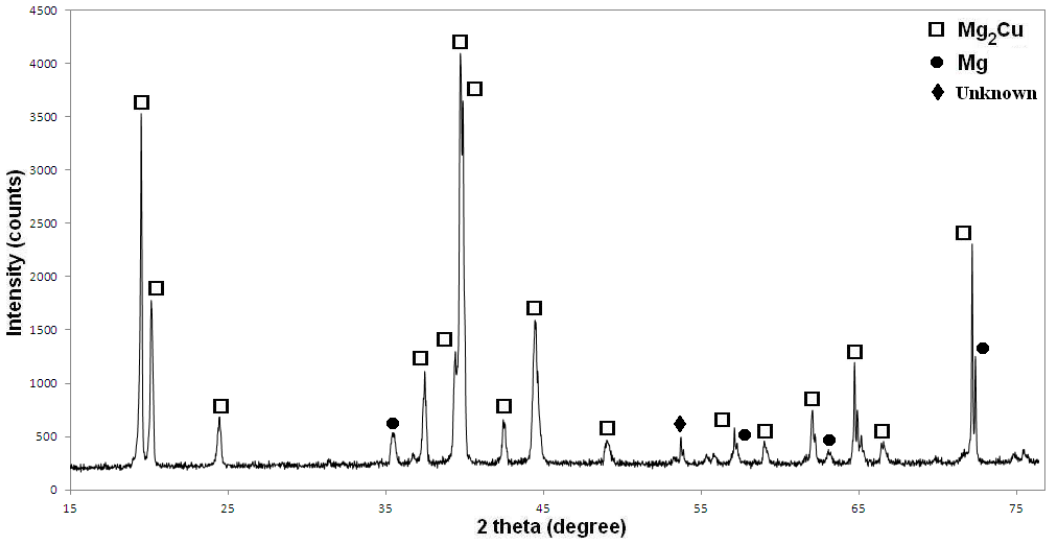

Figure 4.9 XRD diffractogram of the as-solidified Mg_2Cu.

Preliminary experiments with Mg_2Cu showed that hydrogenation cycles were not as easy to apply as was the case in Mg_2Ni. Samples could be hydrogenated with hydrogen at 35 bar, but the rate was rather slow. For this reason experiments were conducted with a slow rate together with a pressure change during absorption and desorption as depicted in Figure 4.10. Heating and cooling rate was 0.5 °C/min. In order to allow desorption from the sample it was necessary to reduce the pressure over the sample. Absorption was initiated at 350 °C and 35 bar by increasing the pressure and the desorption was initiated at room temperature by decreasing the pressure to 1 bar.

Having determined the conditions of cycling, a continuous experiment was carried out for a total of 10 cycles. Absorption and desorption curves recorded are given in Figure 4.11. Following this experiment 10 g of sample was prepared for the interrupted experiment and similar to Mg_2Ni, samples were removed from the reactor after 1^{st}, 3^{rd}, 5^{th}, 7^{th} and 10^{th} cycles. Pressure changes recorded during cycling are given in Figure 4.12 in the form of arbitrary units.

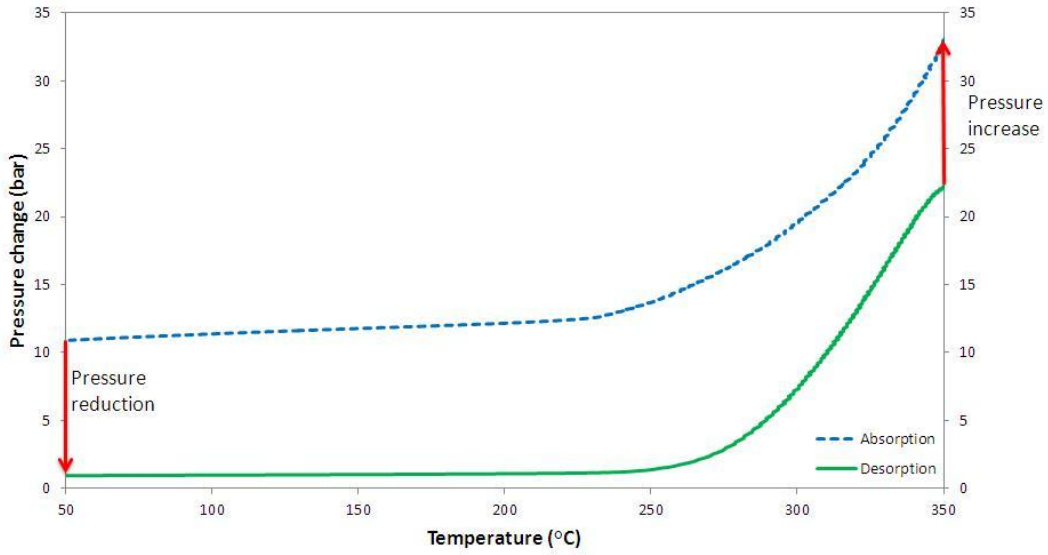

Figure 4.10 Typical hydrogenation cycle for Mg_2Cu.

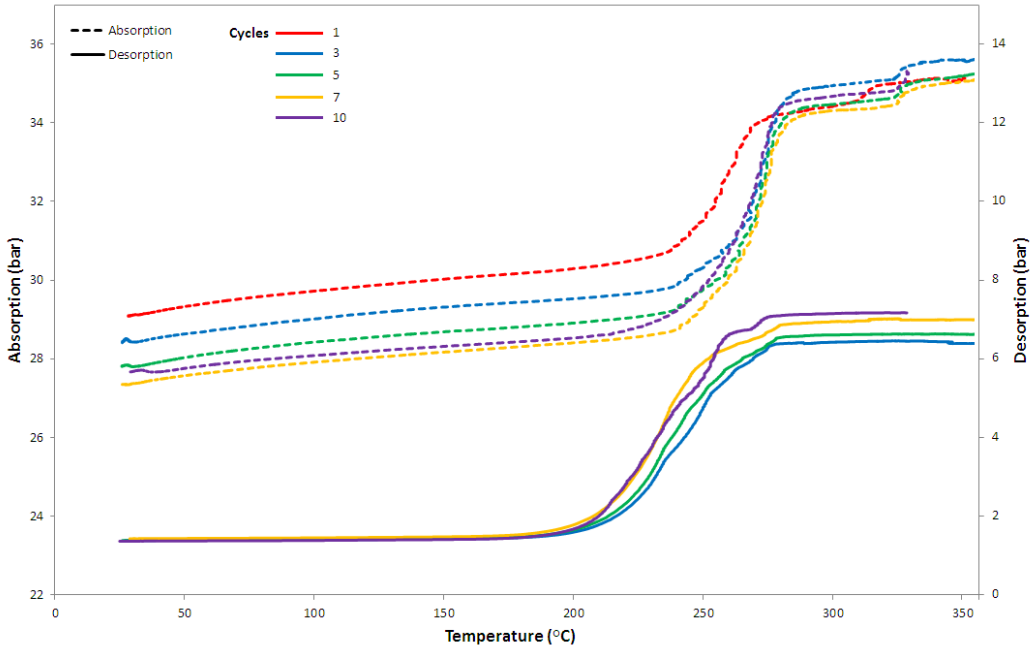

Figure 4.11 Pressure drop and pressure rise versus temperature curves for 10 cycles hydrogenation in Mg_2Cu.

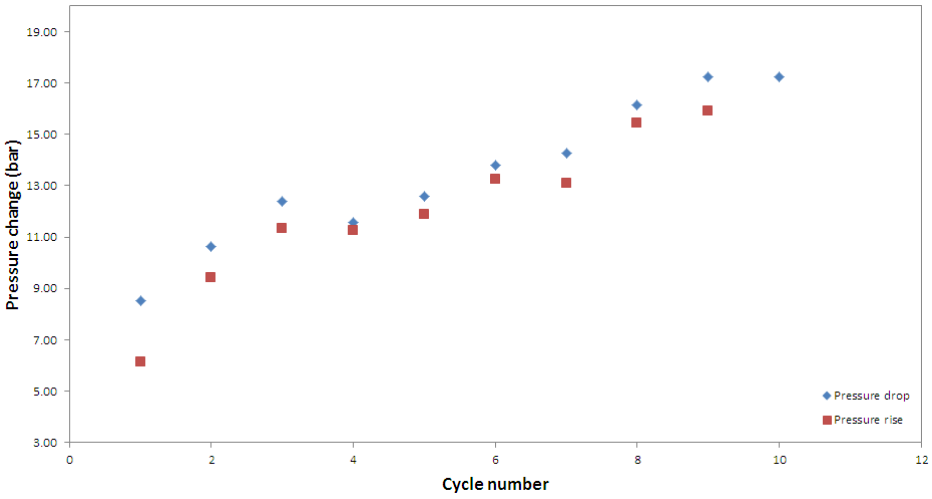

Figure 4.12 Pressure drop at room temperature and pressure rise at 350 °C in Mg_2Ni with cycling.

Particle sizes and surface areas determined for samples removed from the reactor after the cycles stated above are given Table 4.2. Here the values measured with laser diffraction as well as those of BET analysis are given. The values given also include particle size values derived from BET measurement. Here the conversion was made assuming that the particles were spherical in shape and using the density values of 5.11 g/cm^3, 1.45 g/cm^3 and 5.75 g/cm^3 for Mg_2Cu (Gingl et al. 1993), MgH_2 (Lide 2006) and $MgCu_2$ (Muller 2007) respectively. The density of the hydrogenated sample was taken as 2.52 g/cm^3. As seen in Figure 4.13 particle sizes measured by laser diffraction were little affected by cycling. The same is also true for BET measurements though there are considerable scatter in the measured values.

Table 4.2 Surface area values obtained by BET analysis together with particle size values determined by laser diffraction technique and BET analysis for Mg_2Cu.

Cycle number	**Particle size (µm)-laser Diffraction**	**Surface area (m^2/g)-BET**	**Particle size(µm)-BET**
0	59.7	1.25	0.94
1	57	1.24	1.92
3	59.2	1.21	1.97
5	62.6	2.7	0.88
7	57.3	1.46	1.63
10	58.2	2.42	0.99

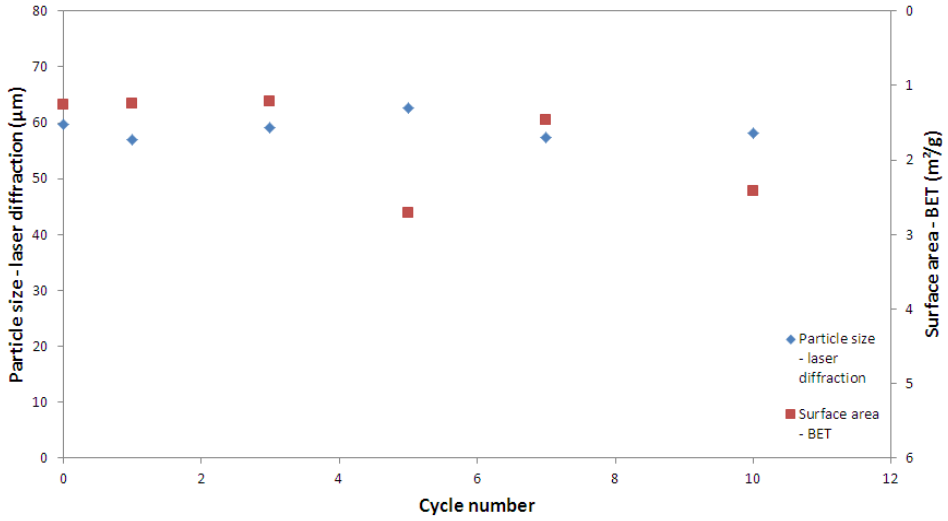

Figure 4.13 Particle sizes calculated by laser diffraction and surface areas determined by BET analysis versus cycle number for Mg_2Cu.

XRD pattern of the sample removed from the reactor after the 10th cycle is given in Figure 4.14. It is seen that the diffractogram are made up of peaks belonging to MgH_2 (JCPDS card no: 72-1687, crystal structure: tetragonal, lattice constants: a= 4.502Å, c= 3.012 Å) and $MgCu_2$ (JCPDS card no: 65-3033, crystal structure cubic, lattice constant: a= 7.048). No Mg_2Cu peak could be observed which implies that the sample was fully hydrogenated.

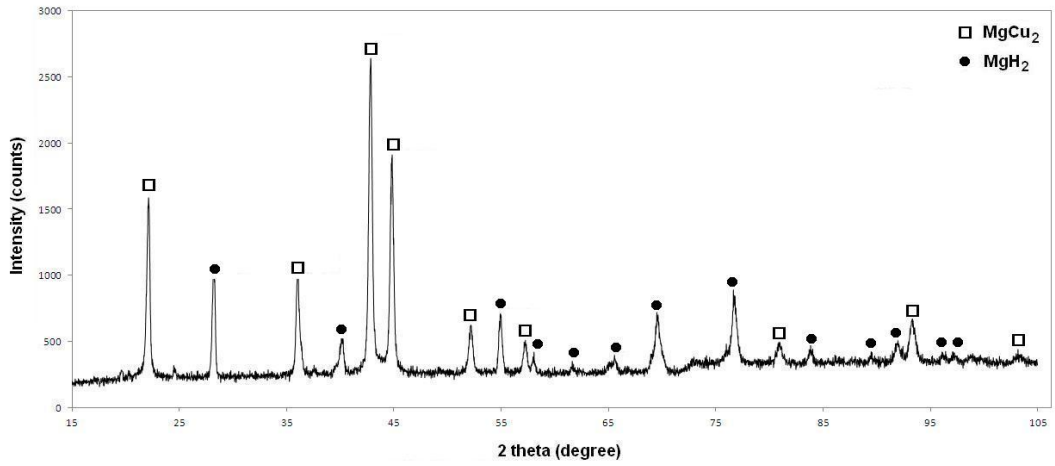

Figure 4.14 XRD difractogram of the hydrided Mg_2Cu.

SEM micrographs of the representative samples are shown in Figure 4.15. Here cycling seems to produce very little effect in the morphology of the Mg_2Cu. Also it is seen that greater portion of particles remained as coarse as the starting material except for the fact that they appear to rounded.

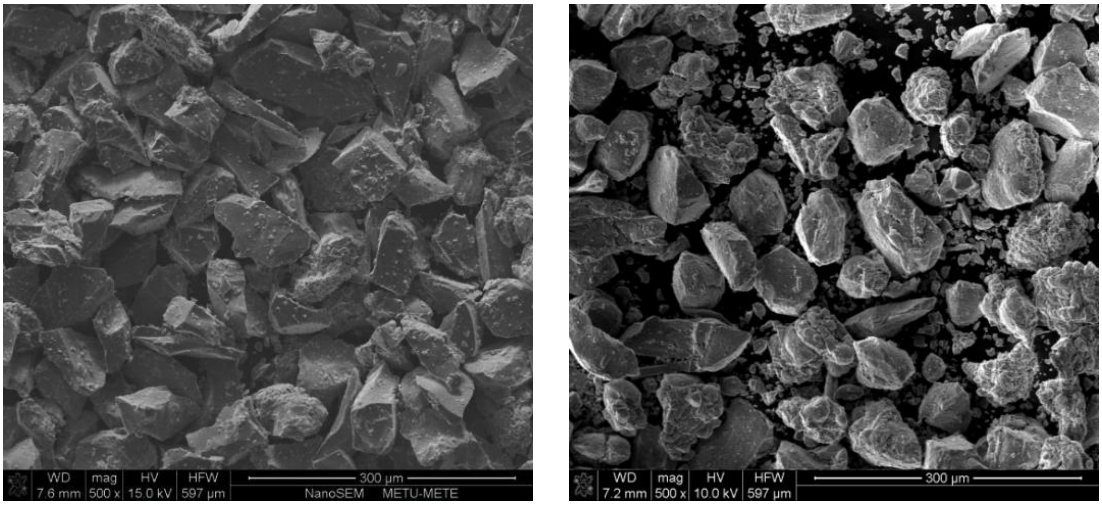

Figure 4.15 SEM images of the Mg_2Cu powder before decrepitation treatment (left) and after the 10^{th} cycle (right).

To examine the dehydrogenated sample, the sample from the 10^{th} cycle was put into the reactor. Following this the reactor was heated up to 350 °C under 1 bar of argon gas and having reached the temperature the reactor was taken under a vacuum ($\approx 10^{-1}$ mbar) for a duration of 10 minutes. Then the reactor was charged with 5 bar of argon and then cooled down to room temperature. The sample was removed from the reactor and exposed to air. XRD pattern recorded from the sample is given in Figure 4.16. It was found that the greater portion of sample was Mg_2Cu as would be expected. There were however additional phases; MgH_2 and $MgCu_2$. The presence of the latter phases implies that dehydrogenation was not complete in the sample.

To investigate the (de)hydrogenation process in detail the samples both in hydrogenated and dehydrogenated state were prepared metallographically by polishing and etching them in using standard metallographic techniques. Figure 4.17 is the hydrided sample where inner portion of the sample appears rather bright as compared to its surrounding. It is believed that the inner portion is the volume which had not dehydrogenated. MgH_2 and $MgCu_2$ observed in the XRD pattern probably originates from these inner portions.

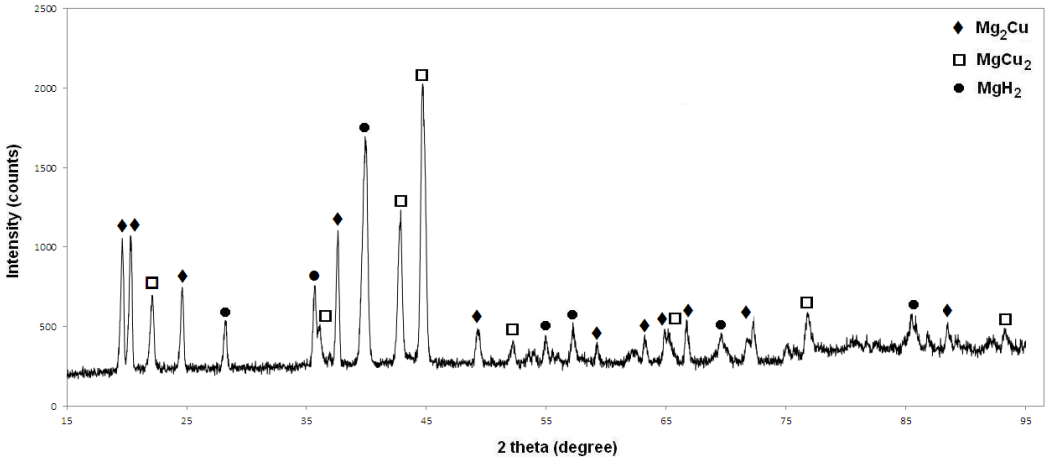

Figure 4.16 XRD difractogram of the dehydrided Mg_2Cu.

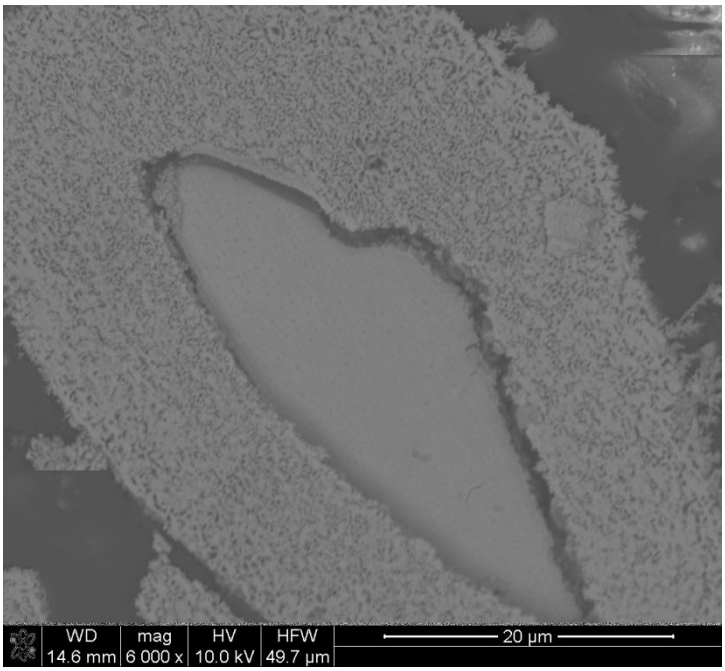

Figure 4.17 Backscattered SEM micrograph of dehydrided Mg_2Cu alloy.

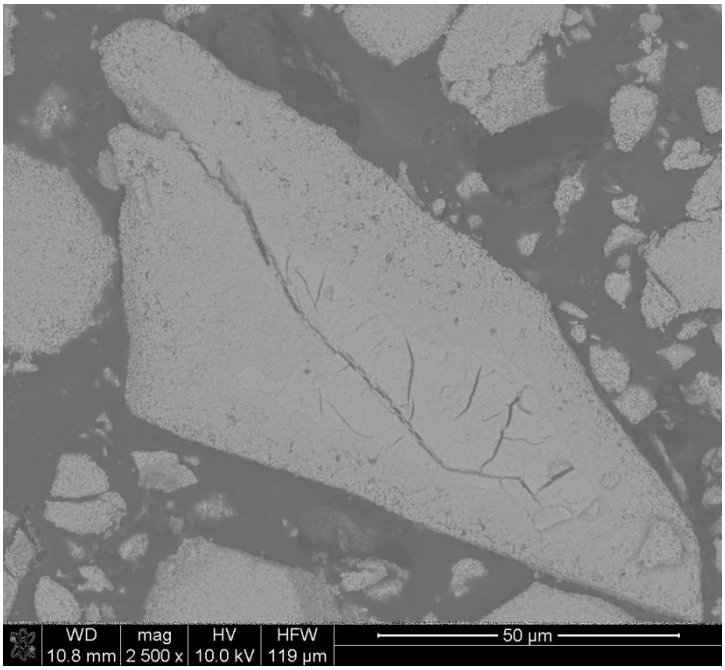

Figure 4.18 Backscattered SEM micrograph of hydrided Mg_2Cu alloy.

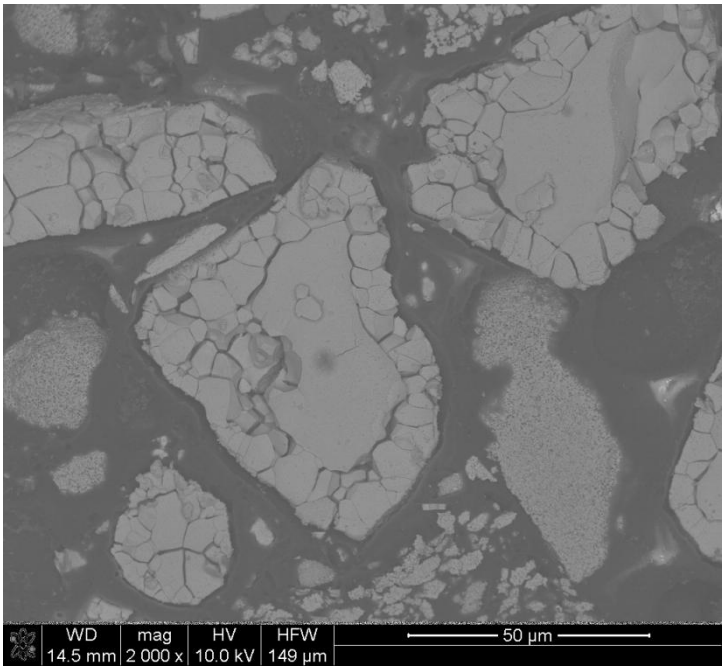

Figure 4.19 Backscattered SEM micrograph of hydrided Mg_2Cu particles which are in the process of fragmentation.

Figure 4.18 refers to hydrogenated sample where a similar occurrence is also noticeable. It appears that the inner portion once hydrogenated in the first cycle remains in the particle but does not take part in the subsequent processes. No quantification was made with regard to particles containing such inner cores, but almost all particles that were large in size e.g. approximately 50 micron had such inner core.

Figure 4.19 refer to smaller particles in the dehydrogenated sample. Here decrepitation process is easily noticeable where the particles are in the process of fragmentation.

4.3 Discussion

This study was focused to production of submicron hydrogen storage alloy particles via hydrogen decrepitation. For this purpose two different intermetallic alloys were selected; Mg_2Ni and Mg_2Cu. These two alloys were investigated whether they are appropriate for hydrogen decrepitation process.

Both alloys were subjected to several hydrogenation/dehydrogenation cycles to observe their pulverization behavior. Mg_2Ni was pulverized significantly after the hydrogenation cycles. With cycling three or more, particles reached sub-micron sizes as verified by SEM examination. In the case of Mg_2Cu, the case is different. Here a greater portion of particles remained with almost the same size as the starting powder.

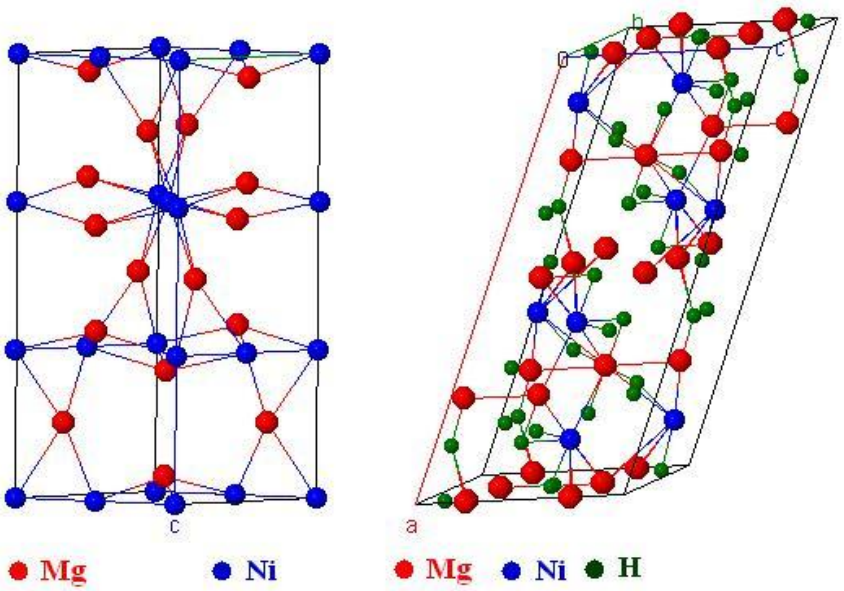

Figure 4.20 Schematic illustrations of the crystal lattices of Mg_2Ni (left) and Mg_2NiH_4 (right).

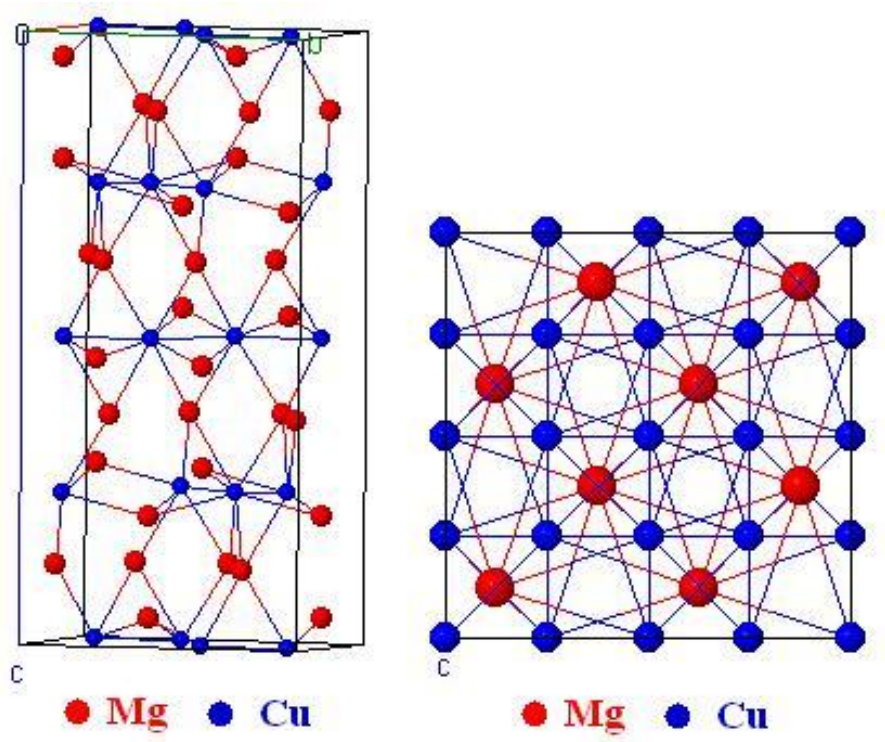

Figure 4.21 Schematic illustrations of the crystal lattices of Mg_2Cu (left) and $MgCu_2$ (right).

Mg_2Ni has a hexagonal crystal structure with lattice parameters of a= 5.21 Å, c= 13.23 Å. Mg_2Ni reacts with hydrogen forming Mg_2NiH_4 (crystal structure: monoclinic, lattice constants: a: 6.496, b: 6.412, c: 13.204). Schematic illustrations of the crystal lattices of both alloys are seen in Figure 4.20. Mg_2Ni reacts with hydrogen with respect to reaction below.

$$Mg_2Ni + 2H_2 \leftrightarrow Mg_2NiH_4 \quad (9)$$

This reaction leads to a lattice expansion of 32.1% upon hydrogenation. Hydrogen decrepitation arises from this rather large volume expansion occurring over a brittle Mg_2Ni intermetallic which therefore flakes off. This observation is in agreement with Semboshi et al. (2001).

When it comes to Mg_2Cu, it reacts with hydrogen in a more complicated way. Rather than direct conversion to hydride, the alloy dissociates into MgH_2 and $MgCu_2$, i.e.

$$2Mg_2Cu + 3H_2 \leftrightarrow 3MgH_2 + MgCu_2 \quad (10)$$

Mg_2Cu has an orthorhombic crystal structure (lattice parameters: a=9.044 Å, b= 5.275 Å, and c= 18.328 Å). MgH_2 has tetragonal crystal structure (lattice constants: a= 4.502Å, c= 3.012 Å) and $MgCu_2$ has cubic crystal structure cubic (lattice constant: a= 7.048). Schematic illustrations of the crystal lattices of Mg_2Cu and $MgCu_2$ are seen in Figure 4.21. Upon hydrogenation the reaction leads to a volume expansion of 24.6%. The value is not too different than that of Mg_2Ni. Despite this volume expansion hydrogenation did not lead to an efficient pulverization.

In conclusion it appears that Mg_2Ni can be processed to sub-micron sizes by applying a several cycles of hydrogenation. Thus this and similar alloys may be processed by decrepitation treatment in which alloys of coarse particle size may be placed into a canister and then are subjected to in-situ decrepitation processing.

Mg_2Cu at least in the conditions prepared in this work is resistant to pulverization and therefore cannot be processed to submicron sizes with decrepitation treatment. SEM micrographs showed that cycling seems to produce very little effect in the morphology of the Mg_2Cu. But particle sizes derived from BET analysis pointed out that the decrepitated powder reached submicron particle size levels. Thus this particle size calculation was considered inaccurate.

The alloy is subject to quite a high volume expansion, comparable to Mg_2Ni. Despite this expansion how the alloy resist pulverization requires further study. This property of the resistance to pulverization may be useful in battery applications.

CHAPTER 5

CONCLUSION

In this study, hydrogen decrepitation was studied in two Mg-rich intermetallics; Mg_2Ni and Mg_2Cu. The alloys were melted under pressure and hand-crushed to coarse sizes and then subjected to decrepitation treatment which consists of hydrogenation and dehydrogenation of the powders in cycles. The treatment was carried out heating and cooling the samples under hydrogen atmosphere.

The followings can be concluded from the present study;

i. Mg_2Ni can be pulverized to submicron sizes with several cycles of hydrogenation and dehydrogenation. Thus the alloy is quite suitable for decrepitation processing.

Therefore this alloy or other alloys of the same type may be just crushed into a coarse powder and could be filled into canister for in-situ pulverization. In contrast to Mg_2Ni;

ii. Mg_2Cu in the condition prepared in this work was resistant to pulverization. Even after 10 decrepitation cycles, the greater portion of the powder was as coarse as the starting powder except for the rounding of sharp corners.

The alloy, therefore, cannot be processed to submicron sizes with decrepitation treatment. This property may be useful in battery applications where the pulverization has a detrimental effect in the cycling performance.

REFERENCES

Akyıldız H., Öztürk T., 2010, Hydrogen sorption in crystalline and amorphous Mg–Cu thin films, Journal of Alloys and Compounds, Volume 492, Issues 1–2, Pages 745-750.

Alcantara R., Audry C., Knosp B., Le Guenne L., Bernard P., 2001, Study of decrepitation and corrosion effects of AB(5) alloys used in Ni/MH batteries by X-ray diffraction, step potential electrochemical spectroscopy and impedance spectroscopy, Journal of New Materials for Electrochemical Systems, Volume 4, Issue 2, Pages 107-114.

Aoki K., Aoyagi H., Memezawa A., Masumoto T., 1994, Effect of ball milling on the hydrogen absorption rate of FeTi and Mg2Ni compounds, Journal of Alloys and Compounds, Volume 203, Pages L7-L9.

Aoyagi H., Aoki K., Masumoto T., 1995, Effect of ball milling on hydrogen absorption properties of FeTi, Mg2Ni and LaNi5, Journal of Alloys and Compounds, Volume 231, Issues 1–2, Pages 804-809.

Arun C., Ramaprabhu S., 1997, Hydrogen absorption studies in Zr0.2Tb0.8Co3 and decrepitation and cyclic stabilities in Zr0.2Tb0.8Co3 and ZrMnFe, Journal of Alloys and Compounds, Volume 259, Issues 1–2, Pages 254-259.

Benjamin J.S., 1970, Dispersion strengthened superalloys by mechanical alloying, Metallurgical Transactions, Volume 1, Issue 10, Pages 2943-&.

Bhatia S.K., Myers A.L., 2006, Optimum conditions for adsorptive storage, Langmuir, Volume 22, Issue 4, Pages 1688-1700.

Bobet J-L., Akiba E., Nakamura Y., Darriet B., 2000, Study of Mg-M (M=Co, Ni and Fe) mixture elaborated by reactive mechanical alloying — hydrogen sorption properties, International Journal of Hydrogen Energy, Volume 25, Issue 10, Pages 987-996.

Çakmak G., Károly Z., Mohai I., Öztürk T., Szépvölgyi J., 2010, The processing of Mg–Ti for hydrogen storage; mechanical milling and plasma synthesis, International Journal of Hydrogen Energy, Volume 35, Issue 19, Pages 10412-10418.

Cocciantelli J.M, Bernard P, Fernandez S, Atkin J, 1997, The influence of Co and various additives on the performance of MmNi4.3−xMn0.33Al0.4Cox hydrogen storage alloys and

Ni/MH prismatic sealed cells, Journal of Alloys and Compounds, Volumes 253–254, Pages 642-647.

Cuevas F., Villeroy B., Leroy E., Olier P., Latroche M., 2007, Relationship between microstructure and hydrogenation properties of Ti0.85Zr0.15Mn1.5V0.5 alloy, Journal of Alloys and Compounds, Volumes 446–447, Pages 218-223.

David E., 2005, An overview of advanced materials for hydrogen storage, Journal of Materials Processing Technology, Volumes 162–163, Pages 169-177.

Dick J.S., 2003, Basic rubber testing: selecting methods for a rubber test program, ASTM International, Pages 107-108.

Eliaz N., Eliezer D., Olson D.L., 2000, Hydrogen-assisted processing of materials, Materials Science and Engineering: A, Volume 289, Issues 1–2, Pages 41-53.

Ewald R., 1998, Requirements for advanced mobile storage systems, International Journal of Hydrogen Energy, Volume 23, Issue 9, Pages 803-814.

Furukawa H., Ko N., Go Y.B., Aratani N., Choi S.B., Choi E., Yazaydin A.O., Snurr R.Q., O'Keeffe M., Kim J., Yaghi O.M., 2010, Ultrahigh porosity in metal-organic frameworks, Science, Volume 329, Issue 5990, Pages 424-428.

Gingl F., Selvam P., Yvon K., 1993, Structure refinement of Mg2Cu and a comparison of the Mg2Cu, Mg2Ni and aAl2Cu structure types, Acta Crystallographica Section B-Structural Science, Volume 49, Part 2, Pages 201-203.

Graetz, J., Reilly, J.J., Nanoscale energy storage materials produced by hydrogen-driven metallurgical reactions, 2005, Advanced Engineering Materials, Volume 7, Issue 7, Pages 597-601.

Harris I.R., Evans J., Nyholm P.S., 1979, British patent 1 554 384.

Harris I.R., McGuiness P.J., 1991, Hydrogen: its use in the processing of NdFeB-type magnets, Journal of the Less Common Metals, Volumes 172–174, Part 3, Pages 1273-1284.

Harris I.R., Noble C., Bailey T., 1985, The hydrogen decrepitation of an Ndi15Fe77B8 magnetic alloy, Journal of the Less Common Metals, Volume 106, Issue 1, Pages L1-L4.

Hirscher M., 2010, Handbook of hydrogen storage : new materials for future energy storage, Wiley-VCH, Page 103.

Hsueh C., Liu C., Chen B., Chen C., Kuo Y., Hwang K., Ku J., 2009, Regeneration of spent-NaBH4 back to NaBH4 by using high-energy ball milling, International Journal of Hydrogen Energy, Volume 34, Issue 4, Pages 1717-1725.

Huot J., Boily S., Güther V., Schulz R., 1999, Synthesis of Na3AlH6 and Na2LiAlH6 by mechanical alloying, Journal of Alloys and Compounds, Volume 283, Issues 1–2, Pages 304-306.

Huot J., Liang G., Schulz R., Mechanically alloyed metal hydride systems, 2001, Applied Physics A-Materials Science & Processing, Volume 72, Issue 2, Pages 187-195.

Huot J., Ravnsbæk D.B., Zhang J., Cuevas F., Latroche M., Jensen T.R., 2013, Mechanochemical synthesis of hydrogen storage materials, Progress in Materials Science, Volume 58, Issue 1, Pages 30-75.

Jiqiao L., Baiyun H., 2001, Particle size characterization of ultrafine tungsten powder, International Journal of Refractory Metals and Hard Materials, Volume 19, Issue 2, Pages 89-99.

Jurczyk M., Okonska I., Iwasieczko W., Jankowska E., Drulis H., 2007, Thermodynamic and electrochemical properties of nanocrystalline Mg2Cu-type hydrogen storage materials, Journal of Alloys and Compounds, Volume 429, Issues 1–2, Pages 316-320.

Kianvash A., Harris I.R., 1985, Hydrogen decrepitation as a method of powder preparation of a 2-17-type, Sm(Co,Cu,Fe,Zr)8.92 magnetic alloy, Journal of Materials Science, Volume 20, Issue 2, Pages 682-688.

Koley S., Ghosh A., Sahu A.K., Tewari R., Suri A. K., 2011, Correlation of compaction pressure, green density, pore size distribution and sintering temperature of a nano-crystalline 2Y-TZP-Al2O3 composite, Ceramics International, Volume 37, Issue 3, Pages 731-739.

Liang G., Boily S., Huot J., Van Neste A., Schulz R., 1998, Mechanical alloying and hydrogen absorption properties of the Mg–Ni system, Journal of Alloys and Compounds, Volume 267, Issues 1–2, Pages 302-306.

Liao J., Huang B., 2001, Particle size characterization of ultrafine tungsten powder, International Journal of Refractory Metals and Hard Materials, Volume 19, Issue 2, Pages 89-99.

Lide D.R., 2006, CRC handbook of chemistry and physics, CRC Press, Edition 87th.

Lin C., Huang S., Jhang Y., 2011, Effects of cyclic hydriding–dehydriding reactions of Mg2Ni alloy on the expansion deformation of a metal hydride storage vessel, Journal of Alloys and Compounds, Volume 509, Issue 25, 23 Pages 7162-7167.

Lowell S., Shields J.E., 1991, Powder surface area and porosity, Springer, Edition 3, Page 18.

Luo J.J., de Rango P., Fruchart D., Mei J.N., Zhou L., 2011, Hydrogen absorption and desorption characteristics of high coercivity NdDyFeCoNbCuB sintered magnet. I. Low temperature hydrogen decrepitation treatments, Journal of Alloys and Compounds, Volume 509, Issue 11, Pages 4252-4259.

Mcguiness P.J., Harris I.R., Rozendaal E., Ormerod J., Ward M., 1986, The production of a Nd-Fe-B permanent-magnet by a hydrogen decrepitation/attritor milling route, Journal of Materials Science, Volume 21, Issue 11, Pages 4107-4110.

Merkus H.G., 2009, Particle size measurements: fundamentals, practice, quality, Springer, Page 13.

Metin O., Mazumder V., Ozkar S., Sun S.S., 2010, Monodisperse nickel nanoparticles; and their catalysis in hydrolytic dehydrogenation of ammonia borane, Journal of The American Chemical Society, Volume 132, Issue 5, Pages 1468-1469.

Miraglia S., de Rango P., Rivoirard S., Fruchart D., Charbonnier J., Skryabina N., 2012, Hydrogen sorption properties of compounds based on BCC Ti1-xV1-yCr1+x+y alloys, Journal of Alloys and Compounds, Volume 536, Pages 1-6.

Mori D., Hirose K., 2009, Recent challenges of hydrogen storage technologies for fuel cell vehicles, International Journal of Hydrogen Energy, Volume 34, Issue 10, Pages 4569-4574.

Muller U., 2007, Inorganic structural chemistry, John Wiley & Sons, Edition 2nd, Page 164.

Murshidi J.A., Paskevicius M., Sheppard D.A., Buckley C.E., 2011, Structure, morphology and hydrogen storage properties of a Ti0.97Zr0.019V0.439Fe0.097Cr0.045 Al0.026Mn1.5 alloy, International Journal of Hydrogen Energy, Volume 36, Issue 13, Pages 7587-7593.

Orimo S., Fujii H., 2001, Materials science of Mg-Ni-based new hydrides, Applied Physics A-Materials Science & Processing, Volume 72, Issue 2, Pages 167-186.

Orimo S., Fujii H., Ikeda K., 1997, Notable hydriding properties of a nanostructured composite material of the Mg2Ni-H system synthesized by reactive mechanical grinding, Acta Materialia, Volume 45, Issue 1, Pages 331-341.

Pasturel M., Wijngaarden R.J., Lohstroh W., Schreuders H., Slaman M., Dam B., Griessen R., 2007, Influence of the chemical potential on the hydrogen sorption kinetics of Mg2Ni/TM/Pd (TM = transition metal) trilayers, Chemistry of Materials, Volume 19, Issue 3, Pages 624-633.

Post M.L., Murray J.J., Despault G.J., Taylor J.B., 1985, The preparation of high-purity Mg2Ni, Materials Research Bulletin, Volume 20, Issue 3, Pages 337-342.

Reilly J. J., Wiswall R. H., 1967, Reaction of hydrogen with alloys of magnesium and copper, Inorganic Chemistry, Volume 6, Issue 12, Pages 2220.

Reilly J. J., Wiswall R. H., 1968, Reaction of hydrogen with alloys magnesium and nickel and formation of Mg2NiH4, Inorganic Chemistry, Volume 7, Issue 11, Pages 2254.

Rhodes M., 2013, Introduction to particle technology, John Wiley & Sons, Edition 2.

Sakintuna B., Lamari-Darkrim F., Hirscher M., 2007, Metal hydride materials for solid hydrogen storage: A review, International Journal of Hydrogen Energy, Volume 32, Issue 9, Pages 1121-1140.

Sandrock G., 1999, A panoramic overview of hydrogen storage alloys from a gas reaction point of view, Journal of Alloys and Compounds, Volumes 293-295, Pages 877-888.

Semboshi S., Masahashi N., Hanada S., 2001, Degradation of hydrogen absorbing capacity in cyclically hydrogenated TiMn2, Acta Materialia, Volume 49, Issue 5, Pages 927-935.

Semboshi S., Masahashi N., Hanada S., 2003, Hydrogenation-induced fragmentation in Ta–Ni alloy, Journal of Alloys and Compounds, Volume 359, Issues 1–2, Pages 236-243.

Semboshi, S., Masahashi, N., Hanada, S., 2004, Hydrogen pulverization of refractory metals, alloys and intermetallics, Metals and Materials International, Volume 10, Issue1, Pages: 45-53.

Shan X., Payer J. H., Wainright J. S., 2006, Increased performance of hydrogen storage by Pd-treated LaNi4.7Al0.3, CaNi5 and Mg2Ni, Journal of Alloys and Compounds, Volume 426, Issues 1–2, Pages 400-407.

Shan X., Payer J. H., Wainright J. S., Dudik L., 2011, A micro-fabricated hydrogen storage module with sub-atmospheric activation and durability in air exposure, Journal of Power Sources, Volume 196, Issue 2, Pages 827-834.

Suh M.P., Park H.J., Prasad T.K., Lim D.W., 2012, Hydrogen storage in metal-organic frameworks, Chemical Reviews, Volume 112, Issue 2-Special Issue, Pages 782-835.

Suresh K., Selvarajan V., Mohai I., 2008, Synthesis and characterization of iron aluminide nanoparticles by DC thermal plasma jet, Vacuum, Volume 82, Issue 5, Pages 482-490.

Suryanarayana C., 2001, Mechanical alloying and milling, Progress in Materials Science, Volume 46, Issues 1–2, Pages 1-184.

Suzuki Y., Haraki T., Uchida H., 2002, Effect of LaNi5H6 hydride particles size on desorption kinetics, Journal of Alloys and Compounds, Volumes 330–332, Pages 488-491.

Szajek A., Jurczyk M., Okońska I., Smardz K., Jankowska E., Smardz L., 2007, Electrochemical and electronic properties of nanocrystalline Mg-based hydrogen storage materials, Journal of Alloys and Compounds, Volume 436, Issues 1–2, Pages 345-350.

Szymczak W., Menzel N., Kreyling W.G., Wittmaack K., 2006, TOF-SIMS characterisation of spark-generated nanoparticles made from pairs of Ir–Ir and Ir–C electrodes, International Journal of Mass Spectrometry, Volume 254, Issues 1–2, Pages 70-84.

Takeshita T., Nakayama R., 1989, Magnetic properties and microstructures of the NdFeB magnet powder produced by hydrogen treatment, Proceedings of the 10th International Workshop on RE Magnet and Their Applications-Kyoto/Japan, Volume 551–557.

Takeshita T., 1995, Some applications of hydrogenation-decomposition-desorption-recombination (HDDR) and hydrogen-decrepitation (HD) in metals processing, Journal of Alloys and Compounds, Volume 231, Issues 1–2, Pages 51-59.

Tsai M., Yeh T., Tsai C., 2006, An improved electrodeposition technique for preparing platinum and platinum–ruthenium nanoparticles on carbon nanotubes directly grown on carbon cloth for methanol oxidation, Electrochemistry Communications, Volume 8, Issue 9, Pages 1445-1452.

Tumas W., Baker R.T., Burrell A., Thorn D., 2006, DOE chemical hydrogen storage center of excellence, DOE Hydrogen Program FY 2006 Annual Progress Report.

Uchida H., Uchida H., Huang Y.C., 1984, Effect of the pulverization of LaNi5 on the hydrogen absorption rate and the X-ray diffraction patterns, Journal of the Less Common Metals, Volume 101, Pages 459-468.

Varin R.A., Czujko T., Wronski Z.S., 2009, Nanomaterials for Solid State Hydrogen Storage Fuel Cells and Hydrogen Energy, Springer.

von Helmolt R., Eberle U., 2007, Fuel cell vehicles: Status 2007, Journal of Power Sources, Volume 165, Issue 2, Pages 833-843.

Wei L., Hervé M., Edouard P., 2012, Use of different rapid mixing devices for controlling the properties of magnetite nanoparticles produced by precipitation, Journal of Crystal Growth, Volume 342, Issue 1, Pages 21-27.

Wenzl H., Klatt K.H., Meuffels P., Papathanassopoulos K. 1983, Hydrogen storage in thin-film metal-hydrides, Journal of the Less-Common Metals, Volume 89, Issue: 2, Pages 489–94.

Westerwaal R.J., Borgschulte A., Lohstroh W., Dam B., Kooi B., ten Brink G., P. Hopstaken M.J., Notten P.H. L., 2006, The growth-induced microstructural origin of the optical black state of Mg2NiHx thin films, Journal of Alloys and Compounds, Volume 416, Issues 1–2, Pages 2-10.

Yadav T.P., Yadav R.M., Singh D. P., 2012, Mechanical milling: a top down approach for the synthesis of nanomaterials and nanocomposites, Nanoscience and Nanotechnology, Volume 2, Issue 3, Pages 22-48.

Yasuda K, 1997, Effects of the materials processing on the hydrogen absorption properties of MmNi5 type alloys, Journal of Alloys and Compounds, Volumes 253–254, Pages 621-625.

Yavari A.R., LeMoulec A., de Castro F.R., Deledda S., Friedrichs O., Botta W.J., Vaughan G., Klassen T., Fernandez A., Kvick Å., 2005, Improvement in H-sorption kinetics of MgH2 powders by using Fe nanoparticles generated by reactive FeF3 addition, Scripta Materialia, Volume 52, Issue 8, Pages 719-724.

Yoshimura H., Nakahigashi J., 2002, Ultra-fine-grain refinement and superplasticity of titanium alloys obtained through protium treatment, International Journal of Hydrogen Energy, Volume 27, Issues 7–8, Pages 769-774.

Yu X.B., Chen J.Z., Wu Z., Xia B.J., Xu N.X., 2004, Effect of Cr content on hydrogen storage properties for Ti-V-based BCC-phase alloys, International Journal of Hydrogen Energy, Volume 29, Issue 13, Pages 1377-1381.

Zakotnik M., Devlin E., Harris I.R., Williams A.J., 2006, Hydrogen Decrepitation and Recycling of NdFeB-type Sintered Magnets, Journal of Iron and Steel Research, Volume 13, Supplement 1, Pages 289-295.

Zaluska A., Zaluski L., Ström–Olsen J.O., 1999, Nanocrystalline magnesium for hydrogen storage, Journal of Alloys and Compounds, Volume 288, Issues 1–2, Pages 217-225.

Zheng J., Liu X., Xu P., Liu P., Zhao Y., Yang J., 2012, Development of high pressure gaseous hydrogen storage technologies, International Journal of Hydrogen Energy, Volume 37, Issue 1, Pages 1048-1057.

Züttel A., 2004, Hydrogen storage methods, Naturwissenschaften, Volume 91, Issue 4, Pages 157-172.